eNeuro

Research Article: New Research | Neuronal Excitability

The structural and electrophysiological properties of progesterone receptor expressing neurons vary along the anterior-posterior axis of the ventromedial hypothalamus and undergo local changes across the reproductive cycle

https://doi.org/10.1523/ENEURO.0049-21.2021

Cite as: eNeuro 2021; 10.1523/ENEURO.0049-21.2021

Received: 7 February 2021
Revised: 6 April 2021
Accepted: 7 April 2021

Title: The structural and electrophysiological properties of progesterone receptor expressing neurons vary along the anterior-posterior axis of the ventromedial hypothalamus and undergo local changes across the reproductive cycle

Abbreviated title: Local hypothalamic changes across the reproductive cycle

Authors: Inês C. Dias[1,2], Nicolas Gutierrez-Castellanos[1,2], Liliana Ferreira[1] & Susana Q. Lima[1]*

1. Champalimaud Research, Champalimaud Centre for the Unknown, Av. Brasilia, s/n Lisboa, Portugal.

2. These authors contributed equally.

* corresponding author: susana.lima@neuro.fchampalimaud.org

Number of pages: 53

Number of figures: 8

Number of tables: 2

Number of words in abstract: 222

Number of words in introduction: 1118

Number of words in discussion: 2243

Conflict of interest statement

The authors declare no competing interests.

Acknowledgments

We thank the Lima Laboratory and Champalimaud Research members for helpful comments on the manuscript, Gil Costa for the graphical abstract design and the Champalimaud Foundation Advanced Bio-optics and Bio-imaging platform for the microscopy technical assistance. This work was supported by the Champalimaud Foundation, Portuguese national funds, through FCT - Fundação para a Ciência e a Tecnologia - in the context of the project UIDB/04443/2020, by the research infrastructure CONGENTO, co-financed by Lisboa Regional Operational Programme (Lisboa2020), under the PORTUGAL 2020 Partnership Agreement, through the European Regional Development Fund (ERDF) and Fundação para a Ciência e Tecnologia (Portugal) under the project LISBOA-01-0145-FEDER-022170, the imagin platform under the project LISBOA-01-0145-FEDER-022122, the project BioData.Pt - LISBOA-01-0145-FEDER-022231 and an ERC Consolidator Grant (772827, SQL).

Abstract

Sex hormone levels continuously fluctuate across the reproductive cycle, changing the activity of neuronal circuits to coordinate female behavior and reproductive capacity. The ventrolateral division of the ventromedial hypothalamus (VMHvl) contains neurons expressing receptors for sex hormones and its function is intimately linked to female sexual receptivity. However, recent findings suggest that the VMHvl is functionally heterogeneous. Here, we used whole recordings and intracellular labeling to characterize the electrophysiological and morphological properties of individual VMHvl neurons in naturally cycling females and report the existence of multiple electrophysiological phenotypes within the VMHvl. We found that the properties of progesterone receptor expressing (PR+) neurons, but not PR- neurons, depended systematically on the neuron's location along the anterior-posterior axis of the VMHvl and the phase within the reproductive cycle. Prominent amongst this, the resting membrane potential of anterior PR+ neurons decreased during the receptive phase, while the excitability of medial PR+ neurons increased during the non-receptive phase. During the receptive phase of the cycle, posterior PR+ neurons simultaneously showed an increase in dendritic complexity and a decrease in spine density. These findings reveal an extensive diversity of local rules driving structural and physiological changes in response to fluctuating levels of sex hormones, supporting the anatomical and functional subdivision of the VMHvl and its possible role in the orchestration of different aspects of female socio-sexual behavior.

67 **Significance Statement**

68 Fluctuating levels of sex hormones coordinate female behavior with their reproductive
69 capacity by acting on neurons expressing their specific receptors. However, it is poorly
70 understood how this seemingly simple message is integrated in local circuits to
71 coordinate complex behavioral responses. Here we show evidence that progesterone
72 receptor expressing neurons of the VMHvl undergo local and specific changes in
73 structure and physiology, suggesting a compartmentalized action of the fluctuating
74 systemic levels of sex hormone across the reproductive cycle, depending on their
75 location in this hypothalamic nucleus.

76

77 **Keywords**: Ventrolateral part of the ventromedial hypothalamus; Progesterone
78 receptor; Structural plasticity; Whole cell recordings; Intrinsic excitability; Reproductive
79 cycle.

80

Introduction

Female reproductive physiology and behavior are under the control of the ovarian sex hormones estrogen and progesterone, whose fluctuating levels act reversibly in the female brain, organizing the activity of neural circuits to synchronize sexual behavior with reproductive capacity (Jennings & de Lecea, 2020; Snoeren, 2018). The ventrolateral division of the ventromedial hypothalamus (VMHvl) is crucial for female reproductive behavior, in particular for the display of lordosis, the female acceptance posture. Non-specific electrolytic lesions (Pfaff & Sakuma, 1979a) or ablation of genetically delineated neuronal populations (Rissman et al., 1997; Yang et al., 2013) of the VMHvl virtually abolish lordosis, while electrical stimulation at the same location enhances the probability of females displaying it (Pfaff & Sakuma, 1979b). Importantly, VMHvl neurons have rich expression of receptors for estrogen (ER) and progesterone (PR) and therefore are sensitive to the fluctuating levels of these sex hormones across the reproductive cycle (Jennings & de Lecea, 2020; Snoeren, 2018). In accordance, local infusion of sex hormones in the VMHvl increases female receptivity (Rubin & Barfield, 1983a) while male-evoked activity in this hypothalamic nucleus is enhanced when females are sexually receptive (Nomoto & Lima, 2015). Moreover, the output of PR-expressing neurons of the VMHvl is altered across the reproductive cycle and this cyclic remodeling is fundamental for the expression of acceptance when females are sexual receptive (Inoue et al., 2019). In summary, vast evidence highlights the importance of the VMHvl for coordinating female's reproductive state with sexual receptivity.

Several studies have shown a large diversity of neuronal types with a wide variety of cellular identities within the VMHvl (Flanagan-Cato, 2011; Kim et al., 2019; McClellan et al., 2006). In addition, the generation of Cre lines providing access to ER- and PR-expressing neurons uncovered further anatomical and functional subdivisions across the nucleus' anterior-posterior axis (AP axis) (Flanagan-Cato, 2011; Hashikawa et al., 2017; Inoue et al., 2019; Kim et al., 2019; Lo et al., 2019; McClellan et al., 2006; Wang et al., 2019), revealing a much broader role of this hypothalamic region in the control of different aspects of female socio-sexual behavior. While regulation of female sexual receptivity seems to be localized to the most posterior-lateral part of the VMHvl, its posterior-medial division is involved in aggressive behavior towards intruders in mothers (Hashikawa et al., 2017). Moreover, it was recently shown that ER-expressing neurons in the anterior portion of the VMHvl are important for self-defense in males (Wang et al., 2019). The connectivity of ER-expressing neurons also varies across the AP axis, further supporting the idea of topographic heterogeneity within this small nucleus (Lo et al., 2019).

How fluctuating levels of sex hormones affect the properties and function of VMHvl neurons remains poorly understood. Most studies aimed at elucidating the impact of sex hormones on neuronal activity in this region have focused on the structural properties of VMHvl neurons. The majority of neurons in the VMHvl have a long primary dendrite (LPD) that extends outside the nucleus, receiving inputs from other forebrain regions, a short primary (SPD), and secondary dendrites that may integrate local inputs (Calizo & Flanagan-cato, 2000; Millhouse, 1973). Previous studies in rodents have shown that externally primed estradiol treatment shortens LPDs and reduces dendritic density in

the VMHvl, effects which are reversed by progesterone (Griffin et al., 2010; Griffin & Flanagan-Cato, 2008). In addition, externally applied ovarian hormones increase the density of dendritic spines on the SPD of VMHvl neurons (Calizo & Flanagan-cato, 2000), and decrease the spine density on the LPD of VMHvl neurons (Calizo & Flanagan-cato, 2002). Moreover, treatment with estrogen was found to lead to an increase in the size of neuronal somata in the VMHvl (Carrer & Aoki, 1982; Griffin & Flanagan-cato, 2011). More recently, it was shown that elevation in the concentration of circulating estrogen increases the number of axon terminals of PR-expressing VMHvl neurons that project to the anteroventral periventricular nucleus of the hypothalamus in female mice and that this plasticity is necessary for sexual receptivity (Inoue et al., 2019). Interestingly, aggressive behavior in males correlates with androgen levels in circulation and is dependent on the physiological and structural plasticity of ER-expressing neurons in the VMHvl (Stagkourakis et al., 2020). However, the electrophysiological properties of VMHvl neurons across the reproductive cycle have received very little attention (but see Kow and Pfaff, 1985 and Booth and Wyman, 2010).

A noteworthy common factor among the vast majority of previous studies on the effects of sex hormones on VMHvl neurons and behavior is that they have been performed in ovariectomized females in which sex hormones were systemically administered at concentrations that do not always match the physiological levels that are observed in naturally cycling females (Liu & Shi, 2015). Moreover, despite the growing evidence suggesting anatomical and functional diversity of the VMHvl, most studies have been largely focused on its most posterior levels (Hashikawa et al., 2017; Inoue et al., 2019;

Yang et al., 2013). However, the VMHvl extends slightly more than a millimeter across the base of the hypothalamus (Kim et al., 2019; Lo et al., 2019), and sex hormone receptor expressing neurons are homogeneously distributed throughout (Kim et al., 2019; Sá & Fonseca, 2017). If and how the structural and physiological properties of VMHvl neurons along its AP axis vary across the female reproductive cycle remains elusive.

In order to gain a more complete understanding of the function of the VMHvl, in the present study we investigated the structural and electrophysiological properties of genetically delineated neurons along the VMHvl AP axis and across the reproductive cycle of naturally cycling females. We focused our efforts on neurons expressing the progesterone receptor, as they are fundamental for female sexual behavior (Yang et al., 2013). To do so, we obtained slices from receptive and non-receptive females and performed in vitro whole-cell recordings of PR expressing (PR+) and PR non-expressing (PR-) neurons, with subsequent reconstruction of the recorded neurons to characterize their electrophysiological and structural properties.

Here we report the existence of multiple electrophysiological phenotypes within the VMHvl and a wide variety of structural and physiological properties across the AP axis of the VMHvl, which are specific for PR+ neurons and that vary locally across the reproductive cycle. For instance, the membrane resting potential of anterior PR+ neurons decreases during the receptive phase, while the excitability of medial PR+ increases when females are non-receptive. During the receptive phase of the cycle, posterior PR+ neurons simultaneously undergo an increase in dendritic complexity and a decrease in spine density. These findings reveal an extensive diversity of local rules

driving structural and physiological changes in response to fluctuating levels of sex hormones, supporting the anatomical and functional subdivision of the VMHvl and its possible role in the orchestration of different aspects of female socio-sexual behavior.

Materials and Methods

Animals

Data was collected from adult PR-Cre-R26R-EYFP (for short PR-EYFP) female mice (2-9 months). PR-EYFP mice express the Enhanced Yellow Fluorescent Protein (EYFP) in cells expressing progesterone receptor (PR+) using the Cre-lox recombination system. Briefly, these mice result from the cross-breeding of B6129S(Cg)-Pgrtm1.1(Cre)Shah/AndJ75 mice (for short PRCre; JAX stock #017915; Yang et al., 2013), containing the Cre recombinase, which is expressed simultaneously with endogenous PR gene, with B6.129X1-Gt(ROSA26Sortm1(EYFP)Cos/J177 mice (for short R26R-EYFP; JAX stock #006148; Srinivas et al., 2001) that have the EYFP gene following a STOP sequence flanked by loxP. Therefore, in their offspring, heterozygous for both PR-Cre and R26R-EYFP alleles, loxP cassettes are removed by the action of Cre recombinase specifically in cells expressing PR, resulting in EYFP expression.

For the visualization of GABAergic somas, we used double heterozygous mice that resulted from the cross-breeding of B6J.129S6(FVB)-Slc32a1$^{tm2(cre)Lowl}$/MwarJ (for short Vgat-ires-Cre knock-in; JAX stock #028862; Vong et al., 2011) with B6;129S6-Gt(ROSA)26Sor$^{tm9(CAG-tdTomato)Hze}$/J (for short Ai9; JAX stock #007905; Madisen et al., 2010). Using the previously described Cre dependent recombinase method, these mice

194 express the fluorescent marker tdTomato under the promoter of the vesicular
195 transporter of GABA.

196 Animals were kept under controlled temperature of 23 ± 1 °C and photoperiod of
197 reversed 12 h light/dark cycle (light available from 8p.m. to 8a.m.) conditions and group-
198 housed in standard cages with environmental enrichment elements. Food and water
199 were provided *ad libitum*. Females were weaned at 20-21 days of age and group-
200 housed with two to five animals.

201 After reaching 6 weeks of age, females were exposed to adult C57BL/6 male soiled
202 bedding once per week to stimulate the natural reproductive cycle. All procedures were
203 carried out in accordance with the animal protocols approved by the Portuguese
204 National Authority for Animal Health (*Direcção Geral de Alimentação e Veterinária*;
205 DGAV) and the Commission for Experimentation and Animal Welfare of the
206 Champalimaud Centre for the Unknown (*Órgão para o Bem Estar Animal*; ORBEA).
207

208 **Reproductive Cycle Monitoring**

209 To assess the reproductive state of naturally cycling female mice, vaginal cytology
210 samples were collected every morning for at least one entire cycle (four/five consecutive
211 days). This collection was done by vaginal lavage using a pipette (T-210-Y, AXYGEN,
212 with its tip cut): 10µL of 0.01M phosphate-buffered saline (PBS) was gently flushed into
213 the vagina and back out three or four times without touching the vaginal wall to avoid
214 cervical stimulation and pseudopregnancy. The flush containing vaginal fluid was
215 transferred to a glass slide and dried (Caligioni, 2009). Papanicolaou staining was used

to differentiate cells (Bio-Optica protocol) and they were observed under a Zeiss AxioScope A1 brightfield microscope with a 10x objective. The identification of the reproductive cycle phase was done based on the proportion of each cell type in the smear. Proestrus is characterized by nucleated epithelial cells. In estrus the main cells present in the vaginal secretion are cornified squamous epithelial cells, clustered with irregular shape. These start to be replaced by leukocytes during metestrus, being these predominant cells in diestrus (Caligioni, 2009; Pfaus, 1999; Snoeren, 2018). Experiments were performed when females were in proestrus/estrus (sexually receptive) or in diestrus (sexually non-receptive).

Ex vivo **Electrophysiological Recordings**

PR-Cre-EYFP mice were deeply anesthetized with isoflurane and decapitated 1-2 hours after the phase of the cycle identification by pap smearing. This protocol is used by the laboratory for behavioral experiments (Nomoto & Lima, 2015). After decapitation, brains were quickly removed and placed into “ice cold” slicing solution containing (in mM): 0.66 kynurenic acid, 3.63 pyruvate, 2.5 KCl, 1.25 NaH_2PO_4, 26 $NaHCO_3$, 10 D-Glucose, 230 Sucrose, 0.5 $CaCl_2$, 10 $MgSO_4$, and bubbled with 5% CO_2 and 95% O_2. Coronal sections with 300μm containing the VMH were cut using a vibratome (Leica VT1200) in the same “ice cold” slicing solution. Slices were recovered in oxygenated artificial cerebrospinal fluid (ACSF) containing (in mM): 127 NaCl, 2.5 KCl, 25 $NaHCO_3$, 1.25 NaH_2PO_4, 25 D-Glucose, 2 $CaCl_2$, and 1 $MgCl_2$, at 34^{o}C for 30 minutes and stored in the same solution at room temperature before being transferred to the recording chamber.

Whole-cell recordings were made under a SliceScope Pro (Scientifica) microscope with the slices submerged in ACSF. A beam of blue light generated with a LED illumination system (CoolLED, pE300) was passed through an immersion objective (Olympus, 40x) to achieve wide field illumination of the slice. PR+ neurons were identified by their natural fluorescence under the microscope and PR- by the absence of fluorescence. A standard GFP filter cube (Thorlabs) was used to filter EYFP emission. EYFP expression, and therefore fluorescence levels, are independent of the reproductive cycle, as after Cre recombination, the expression of the fluorescent protein is dependent on the rosa locus. Patch recording pipettes (resistance 3-5MΩ) were filled with internal solution containing (in mM): 135 K-Gluconate, 10 HEPES, 10 Na-phosphocreatine, 3 Na-L-ascorbate, 4 MgCl2, 4 Na-ATP, 0.4 Na-GTP (pH 7.2 adjusted with NaOH and osmolarity ~292mOs) and 0.1% of biocytin. Internal solution was filtered with a 0.2µm pore size cellulose acetate filter tip. A Multiclamp 700B amplifier and digitized at 10KHz with a Digidata 1440a digitizer (both from Molecular Devices) were used and the data was filtered online with a 10KHz low-pass filter.

We applied a test-pulse of -10mV for 100ms in voltage-clamp mode at -70mV to monitor membrane capacitance and series resistance. To determine excitability and firing properties, current-clamp experiments were performed at resting potential by applying series of 1000ms current pulses between 0 and 240pA with an increasing interval of 30pA at a frequency of 0.1Hz. Hyperpolarization-activated inward current (Ih current) and rebound firing were measured with a 1000ms current pulse at -90pA. The bridge balance was semi-automatically compensated using Axon pCLAMP 10 (Molecular Devices).

After recording, the pipette was carefully withdrawn from the neurons to allow the resealing of the membrane and the diffusion of biocytin inside the neuron. Slices were then transferred to a multi-well plate containing 4% paraformaldehyde (PFA) for ~1 hour for fixation and then transferred to 0.01M PBS for storage prior to immunostaining.

Histology

To visualize biocytin filling, slices were incubated in streptavidin-Alexa Fluor 488 Conjugate (Invitrogen; concentration: 1:200) with 0.3% Triton X-100 in 0.01M PBS at room temperature for 3 hours in dark. After washing three times with 0.01M PBS for 30 minutes each, sections were mounted in glass slides (Menzel-Glazer), coverslipped (Marienfeld) with Mowiol mounting medium (Sigma-Aldrich) and the edges sealed with clear nail polish. For tissue collection, VGat-Cre-tdtomato mice were deeply anesthetized with a lethal amount of a mixture of 12% of ketamine (Imalgene 1000, Merial) and 8% of xylazine (Rompun 2%, Bayer) in saline solution and perfused transcardially with 0.01M PBS followed by 4% PFA in PBS. The brains were removed, fixated in the 4% PFA solution for ~1 hour and transferred to a 30% sucrose (Sigma-Aldrich) in 0.01M Phosphate-Buffer and 0.1% Sodium Azide (ACROS Organics) to allow cryopreservation. Brains were then frozen and coronal sections with 45µm thickness were obtained from the VMH using a freezing sliding microtome (SM2000R, Leica).
Histological sections and fixed ex vivo brain slices were imaged with a Zeiss LSM 710 confocal laser scanning microscope with a 10x and a 25x magnification objectives.

Electrophysiological Data Analysis

A total of 144 recorded neurons were used in the present study. Please see Table 1 and Figure 1 for the numbers of recorded PR+ and PR- neurons, across the reproductive cycle and AP axis.

The action potentials recorded in current-clamp mode were analyzed with custom-written MATLAB code. Each spike within the spike trains obtained upon current injection were detected and used to determine the firing frequency, interspike interval (ISI), threshold to spike, latency to spike and coefficient of variation calculated at a fixed current injection of 150pA). The coefficient of variation was calculated using the following formula (Holt et al., 1996):

$$CV2 = \frac{2|ISI_{n+1} - ISI_n|}{(ISI_{n+1} + ISI_n)}$$

The rebound action potentials observed after injecting hyperpolarizing currents were obtained using the same method.

The first action potential obtained of each spiking sweep was used to calculate the spike amplitude and spike half-width to prevent frequency dependent artifacts in the spike shape caused by sodium and potassium channel inactivation.

The resting potential was determined by averaging the membrane voltage values before the current injection and the Ih current amplitude was calculated by the difference between the early and late phase of a hyperpolarizing current pulse.

Voltage clamp test-pulses were analyzed using Clampfit 10.7 Software (Molecular Devices, LLC) and access resistance (Ra), membrane resistance (Rm), time constant (τ) and capacitance were calculated. Only neurons with access resistance 1/10th lower

than the membrane resistance were used for analysis. Access resistance was comparable across location, genotype and the phase of the cycle in the present study. The passive membrane properties membrane resistance (Rm), membrane capacitance (Cmem), and membrane time constant (τ) were obtained immediately after membrane rupture, using a square voltage step (-10mV, 100ms). The access resistance was determined by measuring the amplitude of the current response to the command voltage step and the membrane resistance as the difference between the baseline and the holding current in the steady state after the capacitive decay, by applying the ohm's law. The membrane time constant was determined by a single exponential fit of the decay phase in response to the square pulse. An approximation of the capacitance was made by using the formula:

$$\tau = membrane\ capacitance * access\ resistance$$

The PCA-initialized t-distributed stochastic neighbor embedding (tSNE) on the firing rates and its subsequent clustering were performed using the *tsne* and *kmeans* functions of Matlab 2020a.

Neuronal Reconstruction and Image Data Analysis

A total of 180 neurons VMHvl neurons were filled with biocytin in acute slices obtained from PR-EYFP female mice using whole-cell recording pipettes. These slices containing biocytin filled neurons were fixed and stained with streptavidin-Alexa 488 Conjugated for the subsequent reconstruction of neuronal structure. In our hands, the native EYFP signal systematically bleached after slice fixation, being several fold dimmer than the fluorescence obtained with Streptavidin-Alexa 488. Therefore, with our confocal

328 settings, no somatic EYFP signal was obtained despite their spectral overlap. Please
329 refer to Table 2 and Figure 6 for the numbers of filled PR+ and PR- neurons across the
330 reproductive cycle and AP axis.

331 To determine the Bregma coordinate for each reconstructed neuron and ensure that its
332 location fell within the VMHvl, in a separate experiment we first assessed the extension
333 of the VMHvl, taking advantage of the VGAT-tdTomato. The VMH is organized in a core
334 of glutamatergic neurons (Ziegler et al 2002, Yamamoto et al 2018) and a surrounding
335 shell with higher density of GABAergic neurons (Yamamoto et al 2018). Therefore, we
336 assessed the AP extension of the VMH by counting consecutive slices in which the
337 VMH was detectable, as shown by a decrease of the VGAT-tdTomato signal (Fig. 6A)
338 and multiplying by the thickness of the histological slices. A sharp transition from low to
339 high tdTomato fluorescence was observed both in its anterior limit (near the anterior
340 hypothalamus) as well as with its posterior limit (near the premammilary hypothalamus)
341 (data not shown). The extension obtained matched the extension illustrated by the
342 Paxinos Brain Atlas: Anterior limit= 1.05 to posterior limit= 2.06 from Bregma (that is,
343 the VMHvl spans for ~1 mm). For each mouse, we systematically sampled 3
344 consecutive levels of the VMH in slices of 300 microns of thickness. We thus
345 categorized each sampling level as anterior (Bregma -1.05 to -1.30 mm approx.), medial
346 (Bregma -1.30 to -1.65 mm approx.), and posterior (Bregma -1.65 to -2.00 mm approx.)
347 levels of the VMH (Fig. 6B-C). Localization of the reconstructed neurons in the brain
348 was assessed by matching in Adobe Illustrator CS6 (Adobe Systems Incorporated) the
349 confocal images of the neurons with adapted sections from the Paxinos brain atlas
350 (Franklin & Paxinos, 2008). Only the neurons inside the defined boundaries of the

VMHvl were considered for quantification. We used the Simple Neurite Tracer (Longair et al., 2011) package from Fiji/ImageJ software (Schindelin et al., 2012) to analyze the morphological properties and Sholl profiles of the neurons filled with biocytin. The Cell Counter Fiji/ImageJ plugin was used to manually count spines.

Cut and resealed dendrites (identified as a globular thickening in the extreme of a dendrite) were quantified for every neuron and did not reveal significant differences across groups (Number of cut dendrites/total number of dendrites quantified per group for PR+ neurons: 21/126 in anteriorNon-Rec, 19/120 in anteriorRec, 20/116 in medialNon-Rec, 31/151 in medialRec, 26/131 in posteriorNon-Rec and 26/121 in posteriorRec. And for PR- neurons: 26/130 in anteriorNon-Rec, 16/70 in anteriorRec, 19/95 in medialNon-Rec, 15/85 in medialRec, 26/100 in posteriorNon-Rec and 17/100 in posteriorRec). When tested with a Fisher's exact test, neither PR+ nor PR- revealed statistical difference in the proportion of cut dendrites. We thus assume that this unavoidable artifact of our method of neuronal recording and reconstruction did not add any group-specific bias in the structural quantification.

In our hands, as well as in previous studies (Calizo & Flanagan-cato, 2000), the intracellular labeling of VMHvl neurons did not always make their thin axonal process visible, and therefore, the axons identified were not considered for analysis.

Graphs were made using custom made MATLAB code or GraphPad Prism 8 Software.

Statistical Analyses

Statistical analyses were performed using GraphPad Prism 8 Software. Normality of the residuals was tested with the D'Agostino-Pearson omnibus K2 test. When normally

distributed, three-way ANOVA tests were performed to compare groups in different phases of the cycle (D vs PE) vs location in the AP axis (anterior vs medial vs posterior) vs genotype (PR+ and PR- neurons), using the Sidak test to correct for multiple comparisons. In Figure 5E, a two-way ANOVA, with Sidak test for multiple comparisons, was used to investigate the origin of the differences in the location factor that were specific for PR- neurons. In the properties whose residuals did not pass the normality test, a logarithmic or square root transformation was applied and normality was consequently reassessed. As specified in the legend, in the properties that the transformations did not make the residuals become normally distributed, we performed a Kruskal-Wallis test followed by a Dunn's post-hoc test for multiple comparisons.

For Figure 2A-F, a Mixed-effects test with repeated measures, and Figure 7C-H a two-way ANOVA with repeated measures were performed. For Figure 1E-F and 5B and C a Chi-square test was performed, the pairwise comparisons we tested followed the same structure as the one obtained for the three-way ANOVA multiple comparisons. Whisker plots represent median with interquartile range. Error bars represent mean ± SEM. p values were rounded to two decimal places. Significance was noted as *$p<0.05$, **$p<0.01$.

Results

The proportion of tonic and phasic firing PR+ neurons varies across the antero-posterior axis.

In order to investigate the neuronal excitability of PR+ and PR- neurons, we recorded current to voltage input-output response curves (I-V curves) at resting potential in current-clamp mode in acute slices of naturally cycling PR-Cre x EYFP adult female

mice. Briefly, the female reproductive stage was determined by vaginal lavage and slices were obtained from females in the least receptive state (diestrus) and the most receptive state (proestrus/estrus). PR+ neurons were identified by their natural fluorescence under the microscope and PR- by the absence of fluorescence (see Methods for details).

We performed a PCA-initialized t-distributed stochastic neighbor embedding (tSNE) analysis on the I-V curve firing rates obtained for our full sample of recorded PR+ and PR- neurons. To understand how many clusters can be optimally distinguished in the resulting embedded data (Fig. 1A), we performed k-means clustering with a possible number of clusters varying between one and eight. When quantifying the sum of squared distances between each datapoint and its assigned cluster centroid over an increasing number of clusters, we observed a characteristic “elbow” shape when there were three possible clusters, suggesting this is the optimal number of clusters in our dataset (Fig. 1B). The first two clusters corresponded to tonic neurons with high and low firing rates (Fig. 1A, A1 and A2, respectively). Tonic firing neurons exhibited a linear increase in firing rate in response to the increases in the magnitude of current injected (Fig. 1C, top). The third cluster roughly corresponded to phasic firing neurons (Fig. 1A, A3), neurons in which the action potentials did not linearly increase in response to increased current injection (Fig. 1C, bottom). These neurons exhibited a step function-like behavior, where after reaching the firing threshold, the number of action potentials remained constant with increased amounts of current. However, when visually inspecting the firing profiles of neurons in this cluster (Fig. 1C), we observed that this cluster included phasic neurons and neurons in which the firing rate initially increased

linearly but then entered depolarization block and drastically reduced their firing rate (Fig. 1A, A4). When dividing the peak firing rate of each neuron by their firing rate at the maximum current injected (240pA), a subset of neurons with particularly high ratio values was clearly distinguishable from the rest (Fig. 1D). These neurons were tonic firing neurons with depolarization block.

We therefore considered two major categories of neurons. The first category being tonic firing neurons, comprising neurons that did not reach the depolarization block within the range of currents we injected (Fig. 1A1 and A2, tonic neurons), and neurons that did (Fig. 1A4, tonic neurons with depolarization block), independently of their firing rate. And the second category being phasic firing neurons (Fig. 1A3).

The majority of the anterior and medial PR+ neurons displayed tonic firing, while most of the posterior ones displayed phasic firing (Fig. 1E, Chi-square test, $p<0.001$), with no differences across the reproductive cycle. In contrast, the PR- population is homogenously composed of a higher proportion of tonic firing neurons across the AP axis (Fig. 1F).

To summarize, the VMHvl is composed of multiple electrophysiological phenotypes and posterior PR+ neurons have a higher density of phasic neurons in comparison to the anterior and medial levels of the VMHvl.

Local changes in the intrinsic excitability and threshold to spike of PR+ neurons across the reproductive cycle.

442 The analysis of the I-V curves revealed that in the anterior and posterior VMHvl, the
443 excitability of PR+ neurons does not to change across the cycle (Fig. 2A and C). In
444 contrast, medial PR+ neurons of non-receptive females showed significantly higher
445 excitability when compared to the excitability of medial PR+ neurons originating from
446 receptive females, particularly in response to higher input current (Fig. 2B, top, strong
447 interaction between the phase of the cycle and the amount of current injected (Mixed-
448 effects test, $F(8, 160)=6.87$, $p<0.0001$)). This modulation is caused by a change in the
449 excitability of the tonic firing medial neurons across the reproductive cycle while the
450 behavior of medial phasic neurons remained unchanged (Fig. 2B, bottom). In addition,
451 this change was specific to the PR+ population since no changes were observed across
452 the cycle in the PR- neurons at any of the AP levels (Fig. 2D-F).
453
454 We also observed that the PR+ population was less excitable than the PR- in the
455 anterior and posterior levels of the VMHvl (Mixed-effects test, ant PR+ vs ant PR- $F(8,$
456 $360)=3.53$, $p<0.001$ and post PR+ vs post PR- $F(8, 361)=2.83$, $p<0.01$) but not in the
457 medial subdivision, probably in part due to the increased excitability of medial PR+
458 neurons from non-receptive females.
459 It is worth mentioning that the membrane resistance did not vary across experimental
460 groups (Table 1) and only a small decrease was observed in the capacitance of the
461 anterior and posterior PR+ of non-receptive females (three-way ANOVA, location/phase
462 interaction $F(2, 132)=3.20$, $p=0.04$). The membrane time constant (τ) also did not vary
463 across the reproductive cycle, however posterior PR+ neurons exhibited a smaller τ

464 when compared to the anterior PR+ population (three-way ANOVA, location $F(2, 132)=3.23$, $p=0.04$, multiple comparison ant vs pos $p=0.04$).

466 The resting potential of anterior PR+ neurons of receptive females was lower when compared to non-receptive females (Fig. 3A and B, three-way ANOVA, phase $F(1,132)=6.39$, $p=0.01$, multiple comparison antNon-Rec vs antRec $p<0.01$). However, this difference was not large enough to produce changes in the threshold to spike (Fig. 3C). The latency to spike of PR+ and PR- neurons did not vary across the cycle (Fig. 3F and H). In addition, we observed a mild, yet significant, lower latency to spike of the posterior neurons when compared to anterior (Fig. 3F and H, three-way ANOVA, location $F(2,132)=5.48$, $p<0.01$, multiple comparison ant vs pos $p=0.01$) and medial neurons (multiple comparison med vs pos $p=0.01$) that was independent of the phase of the cycle and the genotype.

476 The regularity of the recorded spike trains was similar across experimental groups, as shown by comparable CV2 values across phase and location for both the PR+ and PR- populations (regularity was determined at 150pA of injected current, Fig. 3G and I).

479

480 In focusing on the action potential shape, we observed a comparable amplitude and half-width of the action potentials across the reproductive cycle in PR+ and PR- neurons (Fig. 4A-E). The spike amplitude of the posterior neurons of both PR+ and PR- populations is moderately but consistently smaller compared to anterior neurons (Fig. 4B and D, three-way ANOVA, location $F(2,132)=5.74$, $p<0.01$, multiple comparison ant vs pos $p=0.03$) and medial (multiple comparison med vs pos $p<0.01$).

486

Together, these results suggest that the electrophysiological properties of VMHvl neurons vary across the reproductive cycle, but the observed changes depend on their location in the AP axis. In the sexually receptive phase, anterior PR+ neurons are more hyperpolarized in their resting state and the medial PR+ population exhibits lower excitability.

The anterior VMHvl presents a higher proportion of rebound firing neurons during the non-sexually receptive phase of the cycle.

Finally, and given that it is well established that hyperpolarizing input can trigger rebound depolarizing responses increasing the firing rate of neurons in a wide variety of brain areas including the hypothalamus (Burdakov et al., 2004; Israel et al., 2008), we sought to characterize the response of VMHvl neurons to hyperpolarizing input. To do so, we quantified the proportion of VMHvl neurons which exhibited rebound firing after hyperpolarization (Fig. 5A, -90pA for 1s). We observed that 6 out of 32 PR+ neurons of non-receptive females and only 2 out of 38 PR+ neurons of receptive females fired rebound action potentials (Fig. 5B). This difference originates mainly from the anterior PR+ neurons (chi-square test, antNon-Rec+ vs antRec+ p=0.01), where 4 out of 11 neurons of non-receptive females displayed rebound firing while in receptive females none of the 13 recorded neurons produced rebound action potentials. Furthermore, no significant differences were observed between PR+ neurons across the AP axis nor between the PR+ and the PR- populations (Fig. 5B and 5C).

Rebound depolarization is caused by the hyperpolarization activated inward current (Ih) which represents a powerful modulator of neuronal firing frequency and timing (Momin

et al., 2008). Thus, we quantified the Ih current amplitude in VMHvl neurons (Fig. 5D and E). A significant difference was obtained in the interaction between location and genotype (three-way ANOVA, location/genotype interaction $F(2, 132)=4.36$ $p=0.01$), that however, was not large enough to yield statistical differences across groups in the multiple comparisons test. To pinpoint the origin of such changes, we analyzed separately PR+ and PR- populations. Our results show that while the Ih magnitude was unchanged across the AP axis for the PR+ population, the anterior PR- neurons have modestly higher Ih magnitude compared to medial and posterior PR- neurons (Two-way ANOVA, location $F(2,68)=6.30$, $p<0.01$, multiple comparison ant vs med $p=0.04$, ant vs pos $p<0.01$), however, these differences are not reflected in a significantly different fraction of rebound anterior PR- neurons compared medial and posterior PR- neurons (Fig. 5C).

To summarize, the proportion of neurons with rebound firing is fairly homogenous in the VMHvl across the reproductive cycle and independently of genotype, with the exception of its most anterior subdivision, where PR+ neurons exhibit cyclical alterations. Given that these changes are not accompanied by a modulation of Ih current, they likely reflect the change in resting membrane potential that drives receptive neurons away from their firing threshold, causing Ih mediated depolarization to fail to produce rebound firing (Fig. 3B, Fig. 5A).

Localized structural plasticity of VMHvl PR+ neurons across the reproductive cycle.

To study the impact of the phase of the reproductive cycle on the morphological properties of VMHvl neurons, we reconstructed and performed morphometric quantifications of the soma area, number of dendrites, primary dendrites and branch points per neuron of PR+ and PR- neurons in different locations across the AP axis of the VMHvl. As previously reported, the VMHvl is primarily composed of glutamatergic neurons, that are surrounded by GABAergic neurons (Yamamoto et al 2018). In fact, the absence of GABAergic somas has been used to delineate the boundaries of the VMH (Jarvie & Hentges, 2012). Taking advantage of mice expressing the fluorescent reporter tdTomato under the promoter of the vesicular transporter of GABA (VGat-tdTomato) (Kaneko et al., 2018) we observed, as expected, lower signal intensity inside the boundaries of the VMH (Fig. 6A) that was consistent across the AP regions of the VMH. The limits obtained with the inspection of GABAergic markers were used to delineate the boundaries of the VMHvl, and ensure that the neurons characterized in this study were indeed within the nucleus (Fig. 6B and C).

The somatic area was unaltered across the reproductive cycle and was not different between the PR+ and PR- populations (Table 2). We observed that PR+ neurons of receptive females exhibit a robust increase in the number of dendrites per neuron across the AP axis (Table 2, three-way ANOVA, genotype/phase interaction $F(1, 173)=7.85$, $p=0.01$), and a higher number of branching points per neuron compared to neurons originating from non-receptive females (Table 2, three-way ANOVA, genotype/phase interaction $F(1, 173)=5.81$, $p=0.02$). The changes across the reproductive cycle are specific for the PR+ population, as they were not observed in PR-

neurons (Table 2). Both in medial PR+ and PR- neurons, independent of the phase of the cycle, we observed a moderately lower number of primary dendrites per neuron, compared to the anterior and posterior neurons which yielded small yet significant differences across the AP axis (three-way ANOVA, location $F(2, 173)=3.14$, $p=0.04$).

Neurons in the VMHvl are characterized by having a long primary dendrite (LPD) that can be several fold longer than its short primary dendrites (SPD) (Calizo & Flanagan-cato, 2002). Therefore, we analyzed LPD and SPD separately (Table 2). While the length of the LPD of PR+ was unchanged across the reproductive cycle, PR- neurons exhibited longer LPDs in non-receptive females (three-way ANOVA, genotype/phase interaction $F(1, 168)=6.67$, $p=0.01$). No overall significant differences were found in the SPD length of PR+ and PR- neurons across the cycle and AP axis. Interestingly, the posterior neurons were shown to have shorter LPDs than the anterior and medial neurons regardless of the phase of the cycle or the genotype (three-way ANOVA, location $F(2, 168)=9.73$, $p<0.0001$). No differences in the length of LPDs and SPDs were found between the PR+ and PR- populations.

In addition to the analysis of dendritic length, we sought to investigate whether the complexity of the dendritic trees was modified across the reproductive cycle. To do so, we used the Sholl method that measures the number of dendritic processes intersections as a function of the radial distance from the soma. No changes were observed in the maximum number of dendritic intersections of PR+ and PR- neurons across the phase of the cycle (Fig. 7A-H) nor across their location in the VMHvl, indicating that these neurons reach comparable maximum complexities in their dendritic trees. Nevertheless, the analysis of the Sholl profiles of these neurons revealed that the

posterior PR+ neurons of non-receptive females had a significantly lower complexity of their dendritic tree (Fig. 7E, repeated measures ANOVA $p<0.0001$) compared to those from females in the receptive phase. In addition, the medial PR- neurons of non-receptive females had a higher complexity than their counterparts in receptive females (Fig. 7G, repeated measures ANOVA $F(40, 136)=3.10$, $p<0.0001$).

The increased complexity observed in the posterior PR+ neurons of females in the receptive phase was large enough to provide differences when tested with the same method specifically in the proximal branching (Fig. 7E, <250µm from the soma), while the increased complexity of the medial PR- neurons of non-receptive females were observed at more distal parts of the soma (240 to 340µm) and were large enough to yield multiple comparisons significant changes (Fig. 7G).

We also observed that medial PR+ neurons have lower dendritic branching than medial PR- neurons (Fig. 7G, repeated measures ANOVA $F(35, 2030)=2.84$, $p<0.0001$), particularly in the distal parts from the soma (320 to 380µm). The posterior PR+ neurons have lower proximal dendritic branching than the posterior PR- neurons (Fig. 7H, repeated measures ANOVA $F(40, 2520)=1.77$, $p<0.01$). These observations indicate that PR+ neurons have a different dendritic complexity proximal to the cell body compared to that of the PR- population, independent of the phase of the reproductive cycle.

To summarize, similarly to what we report for the electrophysiological properties, the structural properties of PR+ and PR- neurons are diverse, with some varying across the AP axis and the reproductive cycle.

Dendritic spine density largely differs between the PR+ and PR- populations.

Previous studies have shown that externally primed estrogen exerts effects on the dendritic spine density of VMHvl neurons that are different depending on the type of dendrite, specifically, an increase in spine density on SPDs of VMHvl neurons (Calizo & Flanagan-cato, 2000) and a decrease of the spine density on LPDs of VMHvl neurons expressing the receptor for estrogen (Calizo & Flanagan-cato, 2002). In order to determine if such modulation of the spine density of VMHvl neurons is present in the physiological range of sex hormone fluctuation, the dendritic spine density of PR+ and PR- neurons was analyzed depending not only on their location in the VMHvl, but also on the primary dendrite category across the reproductive cycle of naturally cycling females. Although overall PR+ and PR- neurons have comparable spine densities on SPDs across the reproductive cycle (Fig. 8A and C) and location, posterior VMHvl neurons in non- receptive females have higher spine density on SPDs compared to posterior VMHvl neurons in the receptive phase resulting in a significant interaction between the phase of the cycle and location within the VMHvl (three-way ANOVA, phase/location interaction $F(2,153)=3.88$, $p=0.02$). Furthermore, the PR+ population has significantly lower spine density on the SPDs than PR- neurons (Fig. 8E, three-way ANOVA, genotype $F(1, 153)=26.21$, $p<0.01$).

Similar to what was observed for the spine densities of SPDs, for LPDs we observed that the posterior VMHvl neurons of receptive females present a decreased spine density compared to posterior neurons from females that were non-receptive, which in the case of LPDs the change is specific to PR+ neurons (Fig. 8B and D, three-way

ANOVA, phase/location/genotype interaction F(2, 150)=4.81, p=0.01, multiple comparison posNon-Rec+ vs posRec+, p=0.01).

In addition, by comparing PR+ with PR- neurons, we observed that PR+ neurons have lower spine density on the LPDs (Fig. 8F, three-way ANOVA, genotype F(1, 150)=7.25, p=0.01).

Altogether, we observed that neurons expressing progesterone receptor have an overall lower spine density when compared to their neighboring PR- neurons. Across the reproductive cycle, posterior PR+ neurons undergo more pronounced structural changes, exhibiting even lower spine density in the receptive phase.

Discussion

We combined whole-cell recordings with labeling of individual neurons to investigate the structural and electrophysiological properties of PR+ and PR- neurons along the AP axis of the VMHvl and across the reproductive cycle of naturally cycling female mice. First, we report the existence of multiple electrophysiological phenotypes within the VMHvl, including tonic firing neurons (with and without depolarization block) and phasic firing neurons. We show that PR+ cells are distinct from PR- in three major aspects: first, due to structural properties (PR+ neurons have lower spine densities in general); second, due to the great extent to which the properties of PR+ neurons vary across the AP axis; and third due to local changes in the properties of PR+ across the reproductive cycle (which are minimal for the PR- population). Our results further support the

existence of subdivisions in the VMHvl and its possible role in coordinating female behavior with the internal reproductive state.

The impact of the reproductive cycle on VMHvl function has been interrogated *in vivo* and *in vitro*, but most studies were performed in females whose ovaries were removed and then supplemented with estrogen and progesterone (Calizo & Flanagan-cato, 2000, 2002; Griffin et al., 2010; Griffin & Flanagan-Cato, 2008; Millhouse, 1973; Rubin & Barfield, 1980, 1983b, 1983a, but see Inoue et al., 2019; Nomoto & Lima, 2015, for examples of naturally cycling studies). While these manipulations are convenient, easing experimental planning and decreasing interindividual variability (with the extra benefit of allowing a reduction in the number of females used), ovariectomized females with hormonal replacement differ substantially from intact females: first, before hormonal replacement the levels of sex hormones are extremely low, as the main source of estrogen and progesterone is absent and second because the hormonal treatment exposes females to concentrations of sex hormones that differ from physiological levels (Liu & Shi, 2015). The expression of hormone receptors, such as the progesterone receptor, are under the control of sex hormone levels as well (MacLusksy & McEwen, 1978), meaning that that the neuronal response is affected at the level of the receiver (receptor) and message (sex hormone). Persistent hormonal replacement of ovariectomized females leads to tumor development (Kordon et al., 1993) further suggesting that the hormonal treatment leads to undesired physiological effects. Finally, the sexual behavior that hormonally treated females exhibits differs from the behavior of naturally cycling females (Zipse et al., 2000), suggesting that the treatment fails to fully recapitulate the effects of natural sex hormones levels. To the

best of our knowledge, this is the first study interrogating the intrinsic properties of neurons across the reproductive cycle of naturally cycling females and therefore the results observed reflect endogenous changes. However, we cannot claim that the changes we observe across the reproductive cycle are an effect of sex hormone levels because those were not directly manipulated. Manipulations with more naturalistic levels of sex hormones or local manipulations in the expression levels of sex hormone receptors should be employed to establish a direct causal link between hormonal levels, the structural and physiological properties of VMHvl neurons and the changes observed.

In the present study we report, for the first time, the existence of different neuronal types in the VMHvl according to their firing pattern. We found tonic and phasic neurons, in both PR+ and PR- populations, intermingled across the AP axis of the VMHvl. However, the presence of phasic neurons was particularly abundant in the posterior VMHvl, where it comprised more than half of the recorded PR+ neurons.

This AP gradient may have strong implications not only for the role of different portions of the VMHvl in controlling behavioral output, but also for the interpretation of activity manipulations, such as the optogenetic control of neural activity. While anterior VMHvl neurons can reach high firing frequencies, posterior phasic neurons present a robust stop of action potential generation after reaching the spiking threshold that does not depend on the current injected in the cell. Importantly, this may be particularly relevant for the interpretation of results where different laser intensities produce diverse behavioral outputs (Kunwar et al., 2015; Lee et al., 2014), as optogenetic activation at

688 particular AP levels may bias the activation of neuronal populations with different
689 intrinsic properties.

690 Other hypothalamic neuronal populations, such as the tuberoinfundibular dopamine
691 neurons (Lyons et al., 2012) or the gonadotropin-releasing hormone neurons (Jarry et
692 al., 1991) present in the tuberal and preoptic hypothalamus, are known to display phasic
693 firing behavior. Furthermore, the presence of intermingled tonic and phasic firing
694 neuronal population has been previously reported in the magnocellular nucleus of the
695 hypothalamus (Israel et al., 2016), where oxytocin neurons show tonic and vasopressin
696 neurons phasic firing behavior. The differential role of tonic and phasic firing neurons in
697 the control of goal directed behaviors (Budygin et al., 2020; Grace et al., 2007) but also
698 in their contributions for encoding stimulus-environment features (Pilkiw et al., 2017)
699 has been widely studied throughout the brain. In addition, it is known that changes in
700 voltage sensitive channels (Suzuki & Rogawskit, 1989), that can be triggered by
701 neuromodulation (Lyons et al., 2012; Valentino & Van Bockstaele, 2015), are able to
702 mediate the dynamic transition between tonic to phasic firing regimes. In the VMHvl,
703 whether tonic and phasic firing neuronal populations, or the dynamic transition between
704 these firing regimes, contribute to different aspects of socio-sexual behavior remains
705 elusive and should be the focus of future studies.

706 Our results indicate that PR+ cells are distinct from their neighbors, a difference that is
707 probably established early in development, and later on by the fact that their intrinsic
708 properties of this population can be directly affected by estrogen and progesterone, as
709 PR+ neurons co-express estrogen receptor (Blaustein & Turcotte, 1985; Hashikawa et
710 al., 2017; Sá & Fonseca, 2017). Interestingly, the properties of PR- neurons were

similar along the AP axis and across the reproductive cycle, with the exception of changes in the dendritic complexity of neurons in the medial VMHvl. This observation may be explained by the fact that not all ER+ neurons co-express progesterone receptor. ER+/PR- neurons were not labeled with our genetic strategy, but their properties are sensitive to fluctuating levels of estrogen (Calizo & Flanagan-cato, 2000, 2002). Intersectional strategies are needed to address this question.

Interestingly, even though anterior PR+ neurons had a comparable excitability profile across the reproductive cycle, the resting potential of neurons in the receptive phase was significantly hyperpolarized. This change in resting potential likely underlies a moderate increase in the threshold to fire in these neurons, which required more current to start generating action potentials. Even if this trend did not reach significant differences with our current statistical power, the visual difference between anterior non-receptive and receptive PR+ neurons can hardly be overlooked (Fig. **3**C). In addition, the anterior PR+ neurons of receptive females do not show hyperpolarized-induced rebound firing. The fact that these neurons have a more hyperpolarized resting potential, thus more distant from the firing threshold, might explain the fact that the same magnitude of Ih current fails to evoke rebound firing in anterior PR+ at the receptive phase (Fig. 5B). We also report a robust increase of the firing rate under same current injections in medial VMHvl neurons obtained from females in the non-receptive phase compared to those in the receptive phase. These changes were not accompanied by changes in capacitance or membrane resistance across the reproductive cycle of medial neurons, thus it is unlikely that the changes in firing rate are caused by differences in the passive propagation of current into the neuron and

734 instead points towards a modulation of voltage sensitive channels in the medial PR+
735 neurons, that may be mediated by progesterone (Scharfman & MacLusky, 2006).
736 Overall, these results suggest that the anterior and medial VMHvl have the potential to
737 generate more action potentials in non-receptive females, which is in seeming
738 disagreement with the enhanced-male evoked responses that we previously observed,
739 at the population level, in the VMHvl of sexually receptive female mice (Nomoto & Lima,
740 2015). However, the results of this study were obtained with extracellular recordings of
741 non-identified neurons and therefore we do not know if they were PR+ or PR-. Also, in
742 the present study, we investigated the intrinsic properties of VMHvl neurons and cannot
743 make any claim regarding the driving input they receive (synaptic and/or
744 neuromodulatory). The VMHvl receives indirect input from the vomeronasal organ,
745 which includes some neurons whose activity is increased in response to male stimuli
746 when females are sexually receptive (Dey et al., 2015). It is conceivable that the
747 enhanced VMHvl activity that we previously observed reflects modifications at the
748 sensory level.

749 It has been previously reported that hormonal treatment in ovariectomized rats reduced
750 the amount and length of secondary dendrites of a non-defined VMHvl neuronal
751 population (Griffin & Flanagan-cato, 2009). Even if in seeming contradiction with our
752 findings, since we report the opposite effect in dendritic complexity and unchanged
753 dendritic lengths, we would like to point out several possible reasons for such
754 difference. First, the changes we observed are specific to the posterior PR+ population
755 (and absent in our sample of PR- neurons), therefore, sampling VMHvl neurons
756 independently of their genotype could have masked a specific plasticity process in

757 posterior PR+ neurons. Second, in our dataset we observed that medial PR- neurons
758 undergo a reduction in dendritic complexity that goes in line with previous reports. Thus,
759 pooling samples from different levels of the VMHvl may mask changes, or alternatively
760 sampling exclusively in a single AP region of the VMHvl could lead to findings that are
761 limited to that level alone, and thus not generalizable to the whole VMHvl. Interestingly,
762 posterior PR+ neurons did not only undergo changes at the level of their dendritic
763 complexity, but also at the level of spine density, which was reduced in the receptive
764 phase specifically in their LPDs. The fact that such dendritic spine changes are specific
765 to LPDs may suggest that some pathway specific plasticity is happening during the
766 reproductive cycle. Even though it has been previously hypothesized that SPDs may
767 preferentially integrate local excitatory inputs, while LPDs may preferentially interact
768 with long range inputs, inhibitory neurons of the shell and neuropeptides (Griffin &
769 Flanagan-cato, 2011; Yamamoto et al., 2018), as of yet, no circuit mapping study has
770 quantitatively explored what is the anatomical origin of the inputs. Thus, both the
771 anatomical origin of those inputs and their possible relevance for the dendritic coding
772 presented here needs to be further investigated. Our findings suggest a modification of
773 the overall synaptic weights that the LPDs and SPDs will have in the dendritic
774 integration for output generation, with a bias towards the inputs contacting SPDs.

775 It is worth noting that while the spine densities we observed are comparable to the ones
776 reported in previous studies (Calizo & Flanagan-cato, 2002), the dendritic lengths we
777 report both for PR+ and for PR- neurons are several fold longer than those previously
778 reported (Calizo & Flanagan-cato, 2002). These changes may be explained by the
779 differences in the technical approaches used to investigate neuronal structure. While

780 previous reports have used fixed histological slices (100-150 microns) filled *a posteriori*
781 with lucifer yellow, in the present study we have used acute slices for *ex vivo*
782 electrophysiological recordings (300 microns), in which neurons were filled with biocytin
783 during their electrophysiological monitoring. Thus, several key differences may explain
784 the contradictory results: first, the thickness of the slice, which could allow us to track
785 dendrites for longer extensions; second, the fact that neurons in acute slices for *ex vivo*
786 recordings reseal their membranes, producing a visible thickening in the extremity of
787 their cut dendrites, thus allowing us to recognize incomplete dendrites with our technical
788 approach.

789 In summary, we have observed a **multiple electrophysiological phenotypes within**
790 **the VMHvl and a** surprising diversity of structural and physiological plasticity processes
791 both along the AP axis of the VMHvl, and across the reproductive cycle, within the
792 genetically defined population of PR+ cells. These findings highlight the repertoire of
793 local plasticity rules across the VMHvl that is probably explained by the different
794 specialized transcriptomic clusters previously characterized across the AP extension of
795 the VMHvl (Kim et al., 2019; McClellan et al., 2006), supporting the existence of
796 subdivisions in the VMHvl and a more complex role of this hypothalamic structure in
797 socio-sexual behavior, which has been recently acknowledged (Hashikawa et al., 2017;
798 Inoue et al., 2019; Sakurai et al., 2016; Wang et al., 2019; Yang et al., 2013). The
799 existence of multiple subdivisions that undergo local changes in response to sex
800 hormone levels hint to the hypothesis that this hypothalamic structure might be able to
801 control a complex and coordinated set of responses in reaction to an ubiquitous
802 message, the systemic levels of sex hormones in circulation, from metabolism to sexual

803 receptivity. This idea is supported by the connectivity of ER+ neurons, which present a
804 high degree of output divergence, with anterior ER+ neurons projecting to pre-motor
805 areas, while posterior ER+ are engaged in amygdalo-hypothalamic loops (Lo et al.,
806 2019). Similar circuit motifs have been described in other hypothalamic nuclei, such as
807 the organum vasculosum of the lamina terminalis (OVLT), where different subnuclei can
808 coordinate a multipronged response in reaction to thirst (Graebner et al., 2015).
809 Altogether, it becomes evident that acknowledging the different neuronal properties
810 within the AP axis of the VMHvl is crucial to have a holistic understanding of its
811 involvement in behavior and further studies with focal manipulations are needed to
812 understand the functional role of observed local properties and their modulation by the
813 reproductive cycle.

814

Legends

Figure 1 - The predominant firing pattern of PR+ neurons varies across the AP axis and differs from the PR- population.

(A) Low-dimensional embedding of VMHvl neurons Input current to output voltage responses (IV curves) using tSNE. Four representative examples of the different firing responses found correspond to tonic neurons with high firing rate (A1), tonic neurons with low firing rate (A2), phasic neurons (A3), and tonic neurons with depolarization block (A4). (B) Sum of squared distances between each data point and its assigned cluster as a function of increasing number of possible clusters. (C,D) Tonic neurons with depolarization block, that initially were largely clustered with the phasic neurons, can be distinguished by obtaining the ratio between the maximum firing rate and the firing rate at the maximum current injected (240pA). (E) The majority of PR+ neurons in the anterior and medial VMHvl display tonic firing, while the posterior PR+ neurons have mainly phasic firing ($p<0.001$), with no changes across the reproductive cycle. (F) The PR- neurons display mainly tonic firing across the whole AP axis and do not change across the reproductive cycle. Chi-square test. **$p<0.01$

Figure 2 – The excitability of medial PR+ neurons changes across the reproductive cycle.

(A-C) Top: Group mean and SEM of Input-output (IV) curves across the reproductive cycle reporting the firing frequency of PR+ neurons after injecting 1000ms current

pulses between 0 and 240pA (30pA steps), reporting changes only in (B) medial PR+ neurons ($F(8, 160)=6.87$, $p<0.0001$, multiple comparison $p=0.02$ at 180pA, $p<0.01$ at 210pA, $p<0.001$ at 240pA). Bottom: Mean of tonic and phasic firing responses per group. Insets: representative recordings of voltage response from PR+ neurons in response to the same current injection. Anterior n=11 NR, n=13 R, Medial n=11 NR, n=12 R, Posterior n=10 NR, n=13 R. (D-F) Input-output (IV) curves across the reproductive cycle reporting no changes in the firing frequency of PR- neurons after injecting 1000ms current pulses between 0 and 240pA (30pA steps). Insets: representative recordings of voltage response from PR- neurons in response to the same current injection. Anterior n=15 NR, n=11 R, Medial n=10 NR, n=13 R, Posterior n=12 NR, n=13 R. (A,C,D,F) PR+ neurons are less excitable than PR- in the anterior and posterior VMHvl ($F(8, 360)=3.53$, $p<0.001$ and $F(8, 361)=2.83$, $p<0.01$, respectively) but not in (B,E) the medial. Mixed-effects test with repeated measures. Mean (±SEM). *p<0.05

Table 1 - Passive membrane properties of the PR+ and PR- populations across the reproductive cycle and the AP axis.

Capacitance: L1*- location/phase interaction $F(2, 132)=3.20$, $p=0.04$; τ: L2*- location $F(2, 132)=3.23$, $p=0.04$. Three-way ANOVA, Sidak correction for multiple comparison. Values expressed as Median (IQR). *p<0.05

T-Tonic neurons; P-Phasic neurons. Values expressed as Median.

Figure 3 – The resting membrane potential of anterior PR+ neurons changes across the reproductive cycle.

(A) Representative membrane voltage recordings from PR+ neurons in response to 30 and 90pA. (B) Anterior PR+ neurons of receptive females have a lower resting potential compared to non-receptive females (phase $F(1,130)=6.39$, $p=0.01$, multiple comparison antNon-Rec+ vs antRec+ $p<0.01$). (C) The threshold to spike, (F) Latency to spike and (G) Regularity of the spike train (CV2) of the PR+ neurons do not change. Anterior n=11 NR, n=13 R, Medial n=11 NR, n=12 R, Posterior n=10 NR, n=13 R. (D) Resting potential, (E) Threshold to spike, (H) Latency to spike and (I) Regularity of the spike train (CV2) do not vary in PR- neurons across the reproductive cycle. Anterior n=15 NR, n=11 R, Medial n=10 NR, n=13 R, Posterior n=12 NR, n=13 R. (F, H) There is a mild lower latency to spike of the posterior neurons independently of the cycle and genotype (location $F(2, 132)=5.48$, $p=0.01$, L* - multiple comparison ant vs pos $p=0.01$ and med vs pos $p=0.01$). (B, D, F, H) Three-way ANOVA, Sidak correction for multiple comparison. (C, E, G, I) Kruskal-Wallis test, with multiple comparisons. Box plots represent medians (± 25-75 percentile). *$p<0.05$, **$p<0.01$. Individual data points are shown per group color coded according their tonic or phasic firing type.

Figure 4 - The spike waveform of PR+ and PR- neurons is consistent across the reproductive cycle.

(A) Illustration of the recording protocol used to quantify action potential properties and representative examples of the average spike waveform illustrating the amplitude and

the half-with (HW). (B, D) The amplitude of the first action potential for each current injection step of the PR+ and PR- neurons does not change across the reproductive cycle, however it differs mildly across the AP axis (location $F(2, 132)=5.74$, $p<0.01$, multiple comparison L* - ant vs pos $p=0.03$ and L** - med vs pos $p<0.01$). (C, E) The spike half-width of PR+ and PR- neurons is consistent across the reproductive cycle and the AP axis. PR+ Anterior n=11 NR, n=13 R, Medial n=11 NR, n=12 R, Posterior n=10 NR, n=13 R. PR- Anterior n=15 NR, n=11 R, Medial n=10 NR, n=13 R, Posterior n=12 NR, n=13 R. Three-way ANOVA, Sidak correction for multiple comparison. Medians (± 25-75 percentile). *$p<0.05$, **$p<0.01$. Individual data points are shown per group color coded according their tonic or phasic firing type.

Figure 5 - The proportion of anterior PR+ neurons with rebound firing changes across the reproductive cycle.

(A) Example of recordings of voltage response at -90pA. Proportion of neurons presenting rebound firing after hyperpolarization of (B) PR+ neurons from non-receptive and receptive females, and from (C) PR- neurons from non-receptive and receptive females. The anterior PR+ neurons of non-receptive females display a significantly higher fraction of neurons with rebound spikes compared to receptive females ($p=0.01$) Chi-square test. (D) The Ih amplitude of the PR+ neurons does not change across the reproductive cycle nor the AP axis, while the (E) Ih amplitude of PR- neurons varies across the AP axis (three-way ANOVA location/genotype interaction $F(2, 132)=4.36$ $p=0.01$, two-way ANOVA for PR-, location $F(2,68)=6.30$, $p<0.01$, multiple comparison L*

- ant vs med p=0.04, L** - ant vs pos p<0.01). Three-way ANOVA and (E) Two-way, Sidak correction for multiple comparison. *p<0.05. Individual data points are shown per group color coded according their tonic or phasic firing type.

Figure 6 – Localization of reconstructed PR+ and PR- neurons across the VMHvl.

(A) Limits of the VMH obtained with the inspection of GABAergic markers across the AP axis. Schematic representation of the reconstructed PR+ Anterior n=19 NR, n=15 R, Medial n=17 NR, n=19 R, Posterior n=20 NR, n=16 R. (B) and PR- Anterior n=16 NR, n=10 R, Medial n=12 NR, n=12 R, Posterior n=15 NR, n=14 R. (C) neurons and their location in the VMHvl and across the AP axis. Scale bar 200μm.

Table 2 - Morphological profile of PR+ and PR- neurons across the reproductive cycle and the AP axis.

Dendrites per neuron: genotype/phase interaction F(1, 173)=7.85, p=0.01; Branch points per neuron: genotype/phase interaction F(1, 173)=8.81, p=0.02. L1*- Primary dendrites per neuron: location F(2, 173)=3.14, p=0.04. L2*- Length of LPDs: genotype/phase interaction F(1, 168)=6.67, p=0.01, location F(2, 168)=9.73, p<0.0001. Three-way ANOVA, Sidak correction for multiple comparison. Values expressed as Median (IQR). *p<0.05

Figure 7 – The dendritic properties of PR+ neurons are differently modulated across the reproductive cycle depending on the location in the AP axis and differ from the PR- population.

(A) Schematic representation of the Sholl analysis of a posterior PR+ neuron of a non-receptive female and a posterior PR+ neuron of a receptive female (The axon, visible in this case, depicted in lighter shade and not considered for analysis). (B) Confocal image of the posterior PR+ neuron of a receptive female depicted in A filled with biocytin and stained with streptavidin-Alexa 488 Conjugated. Scale bar 50μm. Sholl profiles of (C-E) PR+ Anterior n=19 NR, n=15 R, Medial n=17 NR, n=19 R, Posterior n=20 NR, n=16 R and (F-H) PR- neurons Anterior n=16 NR, n=10 R, Medial n=12 NR, n=12 R, Posterior n=15 NR, n=14 R across the reproductive cycle. (E) The posterior PR+ neurons of receptive females show higher proximal complexity than the ones from non-receptive females (distance from soma x phase of the cycle $F(40, 136)=3.10$, $p<0.0001$, multiple comparison $p<0.001$ at 120μm, $p<0.0001$ at 140-160μm, $p<0.01$ at 180-200μm, and $p=0.04$ at 220μm). (G) Medial PR- neurons from receptive females show lower complexity than the ones from non-receptive females (distance from soma x phase of the cycle $F(33, 726)=2.27$, $p<0.0001$, multiple comparison $p=0.03$ in 320-340μm). (G) The medial PR+ neurons have lower distal branching than the medial PR- neurons (distance from soma x genotype $F(35, 2030)=2.84$, $p<0.0001$, G* - multiple comparison $p=0.04$ at 320μm, $p<0.01$ at 340-360μm $p=0.03$ at 380μm) and (H) the posterior PR+ neurons have lower proximal branching than the PR- neurons (distance from soma x genotype $F(40, 2520)=1.77$, $p<0.01$). Two-way ANOVA with repeated measures. Mean (±SEM).

Figure 8 – The spine density of the LPD of posterior PR+ neurons changes across the reproductive cycle.

(A) Spine density of the SPDs Anterior n=15 NR, n=13 R, Medial n=15 NR, n=17 R, Posterior n=15 NR, n=14 R and the (B) LPDs Anterior n=15 NR, n=13 R, Medial n=15 NR, n=17 R, Posterior n=13 NR, n=14 R of PR+ neurons across the reproductive cycle. The spine density of the LPDs of posterior PR+ neurons is reduced in receptive females (multiple comparison p=0.0170, causing a change in the three-way interaction between the phase of the reproductive cycle, the location in the AP axis and the genotype on the LPDs, $F(2, 150)=4.81$, $p=0.01$). (C) Spine density of the SPDs Anterior n=15 NR, n=10 R, Medial n=12 NR, n=17 R, Posterior n=15 NR, n=12 R and the (D) LPDs Anterior n=15 NR, n=10 R, Medial n=12 NR, n=11 R, Posterior n=15 NR, n=12 R of PR- neurons across the reproductive cycle. (E) PR+ neurons have lower spine density on the SPDs (G** - genotype $F(1, 153)=26.21$, $p<0.01$) and also (F) lower spine density on the LPDs (G* - genotype $F(1, 150)=7.25$, $p=0.01$) than the PR- neurons. Three-way ANOVA, Sidak correction for multiple comparison. Medians (± 25-75 percentile). *$p<0.05$. **$p<0.01$

References

Blaustein, J. D., & Turcotte, J. C. (1985). Estradiol-Induced Progestin Receptor Immunoreactivity Is Found Only in Estrogen Receptor-Immunoreactive Cells in Guinea Pig Brain. In R. Gilles & J. Balthazart (Eds.), *Neurobiology: Current Comparative Approaches* (pp. 60–76). Springer-Verlag. https://doi.org/10.1159/000125152

Budygin, E. A., Bass, C. E., Grinevich, V. P., Deal, A. L., Bonin, K. D., & Weiner, J. L. (2020). Opposite Consequences of Tonic and Phasic Increases in Accumbal Dopamine on Alcohol-Seeking Behavior. *IScience*, *23*(3), 100877. https://doi.org/10.1016/j.isci.2020.100877

Burdakov, D., Alexopoulos, H., Vincent, A., & Ashcroft, F. M. (2004). Low-voltage-activated A-current controls the firing dynamics of mouse hypothalamic orexin neurons. *European Journal of Neuroscience*, *20*(12), 3281–3285. https://doi.org/10.1111/j.1460-9568.2004.03815.x

Caligioni, C. (2009). Assessing Reproductive Status/Stages in Mice. *Current Protocols in Neuroscience*, *Appendix 4*. https://doi.org/10.1002/0471142301.nsa04is48.Assessing

Calizo, L. H., & Flanagan-cato, L. M. (2000). Estrogen Selectively Regulates Spine Density within the Dendritic Arbor of Rat Ventromedial Hypothalamic Neurons. *The Journal of Neuroscience*, *20*(4), 1589–1596.

Calizo, L. H., & Flanagan-cato, L. M. (2002). Estrogen-Induced Dendritic Spine Elimination on Female Rat Ventromedial Hypothalamic Neurons That Project to the

Periaqueductal Gray. *The Journal of Comparative Neurology*, *447*(January), 234–248. https://doi.org/10.1002/cne.10223

Carrer, H. F., & Aoki, A. (1982). Ultrastructural changes in the hypothalamic ventromedial nucleus of ovariectomized rats after estrogen treatment. *Brain Research*, *240*(2), 221–233. http://www.ncbi.nlm.nih.gov/pubmed/7104686

Dey, S., Chamero, P., Pru, J. K., Chien, M. S., Ibarra-Soria, X., Spencer, K. R., Logan, D. W., Matsunami, H., Peluso, J. J., & Stowers, L. (2015). Cyclic regulation of sensory perception by a female hormone alters behavior. *Cell*. https://doi.org/10.1016/j.cell.2015.04.052

Flanagan-Cato, L. M. (2011). Sex Differences in the Neural Circuit that Mediates Female Sexual Receptivity. *Frontiers in Neuroendocrinology*, *32*(2), 124–136. https://doi.org/10.1016/j.yfrne.2011.02.008

Franklin, K., & Paxinos, G. (2008). *The Mouse Brain in Stereotaxic Coordinates, Compact: The Coronal Plates and Diagrams*. Elsevier Science. https://books.google.pt/books?id=PjW5HwAACAAJ

Grace, A. A., Floresco, S. B., Goto, Y., & Lodge, D. J. (2007). Regulation of firing of dopaminergic neurons and control of goal-directed behaviors. In *Trends in Neurosciences* (Vol. 30, Issue 5, pp. 220–227). Trends Neurosci. https://doi.org/10.1016/j.tins.2007.03.003

Graebner, A. K., Iyer, M., & Carter, M. E. (2015). Understanding how discrete populations of hypothalamic neurons orchestrate complicated behavioral states. In *Frontiers in Systems Neuroscience* (Vol. 9, Issue AUGUST). Frontiers Media S.A. https://doi.org/10.3389/fnsys.2015.00111

1013 Griffin, G. D., Ferri-kolwicz, S. L., Reyes, B. A. S., Bockstaele, E. J. Van, & Flanagan-
1014 cato, L. M. (2010). Ovarian Hormone-Induced Reorganization of Oxytocin-Labeled
1015 Dendrites and Synapses Lateral to the Hypothalamic Ventromedial Nucleus in
1016 Female Rats. *The Journal of Comparative Neurology*, *518*, 4531–4545.
1017 https://doi.org/10.1002/cne.22470
1018 Griffin, G. D., & Flanagan-cato, L. M. (2009). Sex Differences in the Dendritic Arbor of
1019 Hypothalamic Ventromedial Nucleus Neurons. *Physiology and Behavior*, *97*(2),
1020 151–156. https://doi.org/10.1016/j.physbeh.2009.02.019.Sex
1021 Griffin, G. D., & Flanagan-cato, L. M. (2011). Ovarian Hormone Action in the
1022 Hypothalamic Ventromedial Nucleus: Remodelling to Regulate Reproduction.
1023 *Journal of Neuroendocrinology*, *23*(6), 465–471. https://doi.org/10.1111/j.1365-
1024 2826.2011.02143.x.Ovarian
1025 Griffin, G. D., & Flanagan-Cato, L. M. (2008). Estradiol and Progesterone Differentially
1026 Regulate the Dendritic Arbor of Neurons in the Hypothalamic Ventromedial Nucleus
1027 of the Female Rat(Rattus norvegicus). *Journal of Comparative Neurology*, *510*(6),
1028 631–640. https://doi.org/10.1002/cne.21816.Estradiol
1029 Hashikawa, K., Hashikawa, Y., Tremblay, R., Zhang, J., Feng, J. E., Sabol, A., Piper,
1030 W. T., Lee, H., Rudy, B., & Lin, D. (2017). Esr1+ cells in the ventromedial
1031 hypothalamus control female aggression. *Nature Neuroscience*, *20*(11), 1580–
1032 1590. https://doi.org/10.1038/nn.4644
1033 Holt, G. R., Softky, W. R., Koch, C., & Douglas, R. J. (1996). Comparison of discharge
1034 variability in vitro and in vivo in cat visual cortex neurons. *Journal of*
1035 *Neurophysiology*, *75*(5), 1806–1814. https://doi.org/10.1152/jn.1996.75.5.1806

1036 Inoue, S., Yang, R., Tantry, A., Davis, C. ha, Yang, T., Knoedler, J. R., Wei, Y., Adams,
1037 E. L., Thombare, S., Golf, S. R., Neve, R. L., Tessier-Lavigne, M., Ding, J. B., &
1038 Shah, N. M. (2019). Periodic Remodeling in a Neural Circuit Governs Timing of
1039 Female Sexual Behavior. *Cell*, *179*(6), 1393-1408.e16.
1040 https://doi.org/10.1016/j.cell.2019.10.025
1041 Israel, J. M., Oliet, S. H., & Ciofi, P. (2016). Electrophysiology of hypothalamic
1042 magnocellular neurons in vitro: A rhythmic drive in organotypic cultures and acute
1043 slices. *Frontiers in Neuroscience*, *10*(MAR).
1044 https://doi.org/10.3389/fnins.2016.00109
1045 Israel, J. M., Poulain, D. A., & Oliet, S. H. R. (2008). Oxytocin-induced postinhibitory
1046 rebound firing facilitates bursting activity in oxytocin neurons. *Journal of*
1047 *Neuroscience*, *28*(2), 385–394. https://doi.org/10.1523/JNEUROSCI.5198-07.2008
1048 Jarry, H., Leonhardt, S., & Wuttke, W. (1991). Gamma-Aminobutyric Acid Neurons in
1049 the Preoptic/Anterior Hypothalamic Area Synchronize the Phasic Activity of the
1050 Gonadotropin-Releasing Hormone Pulse Generator in Ovariectomized Rats.
1051 *Neuroendocrinology*, *53*(3), 261–267. https://doi.org/10.1159/000125727
1052 Jarvie, B. C., & Hentges, S. T. (2012). Expression of GABAergic and glutamatergic
1053 phenotypic markers in hypothalamic proopiomelanocortin neurons. *Journal of*
1054 *Comparative Neurology*, *520*(17), 3863–3876. https://doi.org/10.1002/cne.23127
1055 Jennings, K. J., & de Lecea, L. (2020). Neural and hormonal control of sexual behavior.
1056 In *Endocrinology (United States)* (Vol. 161, Issue 10). Endocrine Society.
1057 https://doi.org/10.1210/endocr/bqaa150
1058 Kaneko, R., Takatsuru, Y., Morita, A., Amano, I., Haijima, A., Imayoshi, I., Tamamaki,

N., Koibuchi, N., Watanabe, M., & Yanagawa, Y. (2018). Inhibitory neuron-specific Cre-dependent red fluorescent labeling using VGAT BAC-based transgenic mouse lines with identified transgene integration sites. *Journal of Comparative Neurology*, *526*(3), 373–396. https://doi.org/10.1002/cne.24343

Kim, D. W., Yao, Z., Graybuck, L. T., Kim, T. K., Nguyen, T. N., Smith, K. A., Fong, O., Yi, L., Koulena, N., Pierson, N., Shah, S., Lo, L., Pool, A. H., Oka, Y., Pachter, L., Cai, L., Tasic, B., Zeng, H., & Anderson, D. J. (2019). Multimodal Analysis of Cell Types in a Hypothalamic Node Controlling Social Behavior. *Cell*, *179*(3), 713–728. https://doi.org/10.1016/j.cell.2019.09.020

Kordon, E. C., Molinolo, A. A., Pasqualini, C. D., Charreau, E. H., Pazos, P., Dran, G., & Lanari, C. (1993). Progesterone induction of mammary carcinomas in BALB/c female mice - Correlation between progestin dependence and morphology. *Breast Cancer Research and Treatment*, *28*(1), 29–39. https://doi.org/10.1007/BF00666353

Kunwar, P. S., Zelikowsky, M., Remedios, R., Cai, H., Yilmaz, M., Meister, M., & Anderson, D. J. (2015). Ventromedial hypothalamic neurons control a defensive emotion state. *ELife*, *2015*(4). https://doi.org/10.7554/eLife.06633

Lee, H., Kim, D., Remedios, R., Anthony, T. E., Chang, A., Madisen, L., Zeng, H., & Anderson, D. J. (2014). Scalable Control of Mounting and Attack by ESR1+ Neurons in the Ventromedial Hypothalamus. *Nature*, *509*(7502), 627–632. https://doi.org/10.1038/nature13169

Liu, X., & Shi, H. (2015). Regulation of Estrogen Receptor Expression in the Hypothalamus by Sex Steroids: Implication in the Regulation of Energy

Homeostasis. In *International Journal of Endocrinology* (Vol. 2015). Hindawi Publishing Corporation. https://doi.org/10.1155/2015/949085

Lo, L., Yao, S., Kim, D. W., Cetin, A., Harris, J., Zeng, H., Anderson, D. J., & Weissbourd, B. (2019). Connectional architecture of a mouse hypothalamic circuit node controlling social behavior. *Proceedings of the National Academy of Sciences of the United States of America*, *116*(15), 7503–7512. https://doi.org/10.1073/pnas.1817503116

Longair, M. H., Baker, D. A., & Armstrong, J. D. (2011). Simple Neurite Tracer: open source software for reconstruction, visualization and analysis of neuronal processes. *Bioinformatics (Oxford, England)*, *27*(17), 2453–2454. https://doi.org/10.1093/bioinformatics/btr390

Lyons, D. J., Hellysaz, A., & Broberger, C. (2012). Prolactin regulates tuberoinfundibular dopamine neuron discharge pattern: Novel feedback control mechanisms in the lactotrophic axis. *Journal of Neuroscience*, *32*(23), 8074–8083. https://doi.org/10.1523/JNEUROSCI.0129-12.2012

MacLusksy, N. J., & McEwen, B. S. (1978). Oestrogen Modulates Progestin Receptor Concentrations in Some Rat Brain Regions But Not in Others. In *Nature* (Vol. 274, pp. 276–278). https://doi.org/10.1038/274276a0

Madisen, L., Zwingman, T. A., Sunkin, S. M., Oh, S. W., Zariwala, H. A., Gu, H., Ng, L. L., Palmiter, R. D., Hawrylycz, M. J., Jones, A. R., Lein, E. S., & Zeng, H. (2010). A robust and high-throughput Cre reporting and characterization system for the whole mouse brain. *Nature Neuroscience*, *13*(1), 133–140. https://doi.org/10.1038/nn.2467

1105 McClellan, K. M., Parker, K. L., & Tobet, S. (2006). Development of the ventromedial
1106 nucleus of the hypothalamus. *Frontiers in Neuroendocrinology*, *27*(2), 193–209.
1107 https://doi.org/10.1016/j.yfrne.2006.02.002
1108 Millhouse, O. E. (1973). The Organization of the Ventromedial Hypothalamic Nucleus.
1109 *Brain Research*, *55*, 71–87.
1110 Momin, A., Cadiou, H., Mason, A., & Mcnaughton, P. A. (2008). Role of the
1111 hyperpolarization-activated current Ih in somatosensory neurons. *Journal of*
1112 *Physiology*, *586*(24), 5911–5929. https://doi.org/10.1113/jphysiol.2008.163154
1113 Nomoto, K., & Lima, S. Q. (2015). Report Enhanced Male-Evoked Responses in the
1114 Ventromedial Hypothalamus of Sexually Receptive Female Mice Enhanced Male-
1115 Evoked Responses in the Ventromedial Hypothalamus of Sexually Receptive
1116 Female Mice. *Current Biology*, *25*(5), 589–594.
1117 https://doi.org/10.1016/j.cub.2014.12.048
1118 Pfaff, D. W., & Sakuma, Y. (1979a). Deficit in the Lordosis Reflex of Female Rats
1119 Caused by Lesions in the Ventromedial Nucleus of the Hypothalamus. *The Journal*
1120 *of Physiology*, *288*(1), 203–210. https://doi.org/10.1113/jphysiol.1979.sp012691
1121 Pfaff, D. W., & Sakuma, Y. (1979b). Facilitation of the Lordosis Reflex of Female Rats
1122 From the Ventromedial Nucleus of the Hypothalamus. *The Journal of Physiology*,
1123 *288*(1), 189–202. https://doi.org/10.1113/jphysiol.1979.sp012690
1124 Pfaus, J. G. (1999). Neurobiology of Sexual Behavior. *Current Opinion in Neurobiology*,
1125 *9*(6), 751–758. https://doi.org/10.1016/S0959-4388(99)00034-3
1126 Pilkiw, M., Insel, N., Cui, Y., Finney, C., Morrissey, M. D., & Takehara-Nishiuchi, K.
1127 (2017). Phasic and tonic neuron ensemble codes for stimulus-environment

conjunctions in the lateral entorhinal cortex. *ELife*, *6*. https://doi.org/10.7554/eLife.28611

Rissman, E. F., Early, A. H., Taylor, J. A., Korach, K. S., & Lubahn, D. B. (1997). Estrogen Receptors are Essential for Female Sexual Receptivity. *Endocrinology*, *138*(1), 507–510.

Rubin, B. S., & Barfield, R. J. (1980). *Priming of Estrous Responsiveness by Implants of 17 beta-Estradiol in the Ventromedial Hypothalamic Nucleus of Female Rats*. *106*(2), 504–509.

Rubin, B. S., & Barfield, R. J. (1983a). Induction of Estrous Behavior in Ovariectomized Rats by Sequential Replacement of Estrogen and progesterone to the Ventromedial Hypothalamus. *Neuroendocrinology*, *37*, 218–224.

Rubin, B. S., & Barfield, R. J. (1983b). *Progesterone in the Ventromedial Hypothalamus Facilitates Estrous Behavior in Ovariectomized, Estrogen-Primed Rats*. *113*(2).

Sá, S. I., & Fonseca, B. M. (2017). Dynamics of progesterone and estrogen receptor alpha in the ventromedial hypothalamus. *Journal of Endocrinology*, *233*(2), 197–207. https://doi.org/10.1530/JOE-16-0663

Sakurai, K., Zhao, S., Takatoh, J., Rodriguez, E., Lu, J., Leavitt, A. D., Fu, M., Han, B. X., & Wang, F. (2016). Capturing and Manipulating Activated Neuronal Ensembles with CANE Delineates a Hypothalamic Social-Fear Circuit. *Neuron*, *92*(4), 739–753. https://doi.org/10.1016/j.neuron.2016.10.015

Scharfman, H. E., & MacLusky, N. J. (2006). The influence of gonadal hormones on neuronal excitability, seizures, and epilepsy in the female. *Epilepsia*, *47*(9), 1423–1440. https://doi.org/10.1111/j.1528-1167.2006.00672.x

1151 Schindelin, J., Arganda-Carreras, I., Frise, E., Kaynig, V., Longair, M., Pietzsch, T.,
1152 Preibisch, S., Rueden, C., Saalfeld, S., Schmid, B., Tinevez, J. Y., White, D. J.,
1153 Hartenstein, V., Eliceiri, K., Tomancak, P., & Cardona, A. (2012). Fiji: An open-
1154 source platform for biological-image analysis. In *Nature Methods*.
1155 https://doi.org/10.1038/nmeth.2019
1156 Snoeren, E. M. S. (2018). Female Reproductive Behavior. In *Current topics in*
1157 *behavioral neurosciences*. https://doi.org/10.1007/7854_2018_68
1158 Srinivas, S., Watanabe, T., Lin, C. S., William, C. M., Tanabe, Y., Jessell, T. M., &
1159 Costantini, F. (2001). Cre reporter strains produced by targeted insertion of EYFP
1160 and ECFP into the ROSA26 locus. *BMC Developmental Biology*, *1*(4).
1161 http://www.ncbi.nlm.nih.gov/pubmed/11299042
1162 Stagkourakis, S., Spigolon, G., Liu, G., & Anderson, D. J. (2020). Experience-
1163 dependent plasticity in an innate social behavior is mediated by hypothalamic LTP.
1164 *Proceedings of the National Academy of Sciences of the United States of America*,
1165 *117*(41), 25789–25799. https://doi.org/10.1073/pnas.2011782117
1166 Suzuki, S., & Rogawskit, M. A. (1989). T-type calcium channels mediate the transition
1167 between tonic and phasic firing in thalamic neurons (lateral geniculate nudeus/low-
1168 threshold spike/nickel/dihydropyridine). In *Proc. Nail. Acad. Sci. USA* (Vol. 86).
1169 Valentino, R. J., & Van Bockstaele, E. (2015). Endogenous opioids: The downside of
1170 opposing stress. In *Neurobiology of Stress* (Vol. 1, Issue 1, pp. 23–32). Elsevier
1171 Inc. https://doi.org/10.1016/j.ynstr.2014.09.006
1172 Vong, L., Ye, C., Yang, Z., Choi, B., Chua, S., & Lowell, B. B. (2011). Leptin Action on
1173 GABAergic Neurons Prevents Obesity and Reduces Inhibitory Tone to POMC

Neurons. *Neuron*, *71*(1), 142–154. https://doi.org/10.1016/j.neuron.2011.05.028

Wang, L., Talwar, V., Osakada, T., Kuang, A., Guo, Z., Yamaguchi, T., & Lin, D. (2019). Hypothalamic Control of Conspecific Self-Defense. *Cell Reports*, *26*(7), 1747-1758.e5. https://doi.org/10.1016/j.celrep.2019.01.078

Yamamoto, R., Ahmed, N., Ito, T., Gungor, N. Z., & Pare, D. (2018). Optogenetic Study of Anterior BNST and Basomedial Amygdala Projections to the Ventromedial Hypothalamus. *Eneuro*, *5*(3), 204–218. https://doi.org/10.1523/eneuro.0204-18.2018

Yang, C. F., Chiang, M. C., Gray, D. C., Prabhakaran, M., Alvarado, M., Juntti, S. A., Unger, E. K., Wells, J. A., & Shah, N. M. (2013). Sexually Dimorphic Neurons in the Ventromedial Hypothalamus Govern Mating in Both Sexes and Aggression in Males. *Cell*, *153*(4), 896–909. https://doi.org/10.1016/j.cell.2013.04.017

Zipse, L. R., Brandling-Bennett, E. M., & Clark, A. S. (2000). Paced mating behavior in the naturally cycling and the hormone-treated female rat. *Physiology and Behavior*, *70*(1–2), 205–209. https://doi.org/10.1016/S0031-9384(00)00242-0

Autor contribution

ICD, NG and SQL designed the research. ICD, NG and LF performed the research. ICD and NG analyzed the data. ICD, NG and SQL wrote the paper.

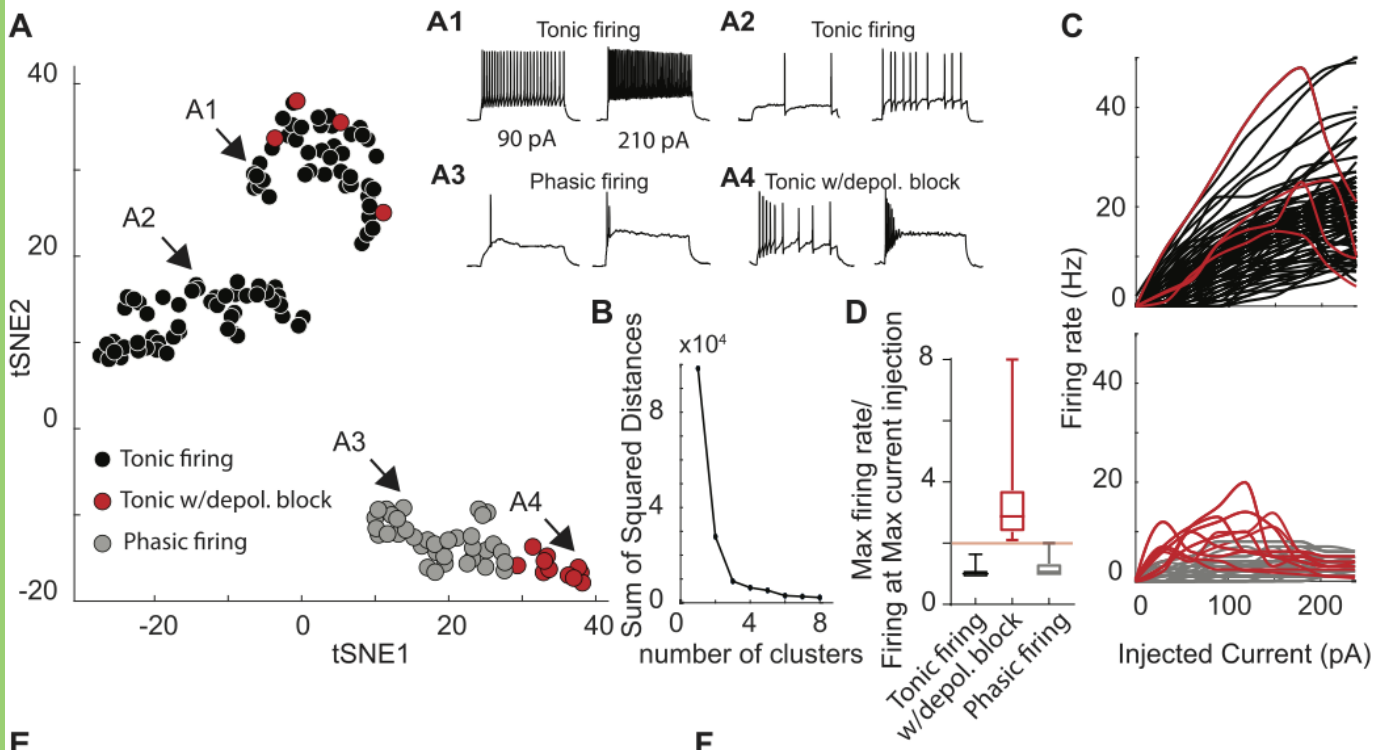

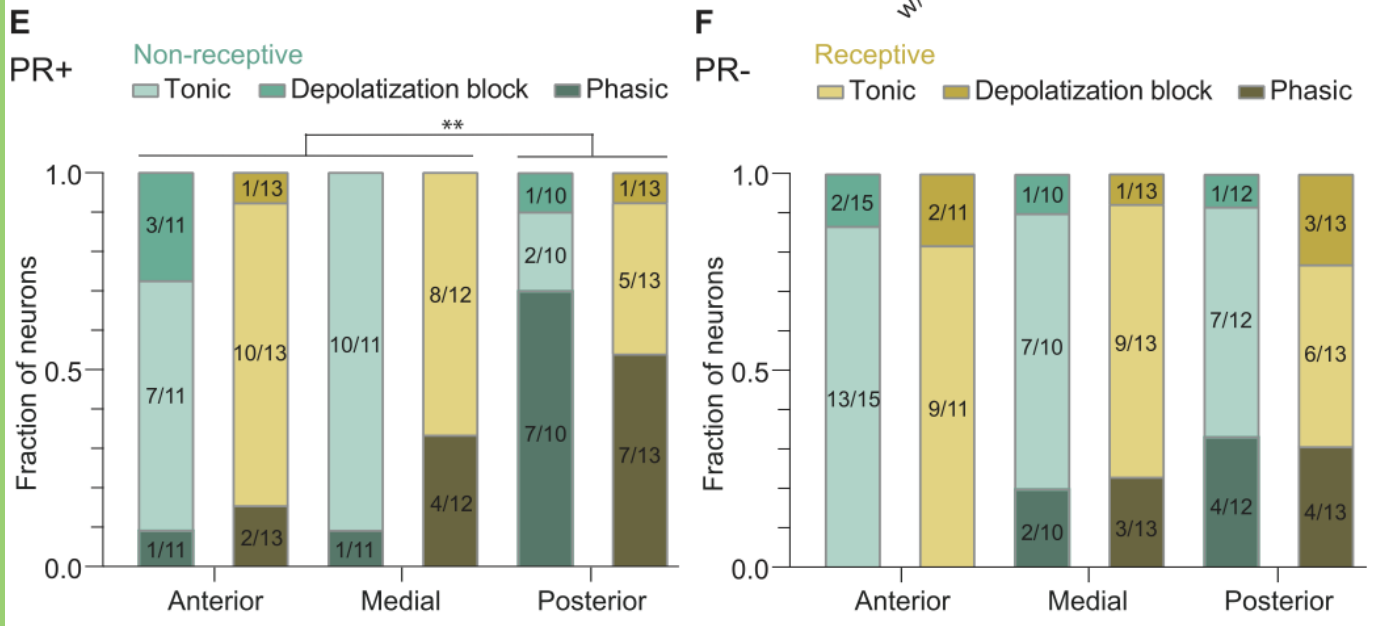

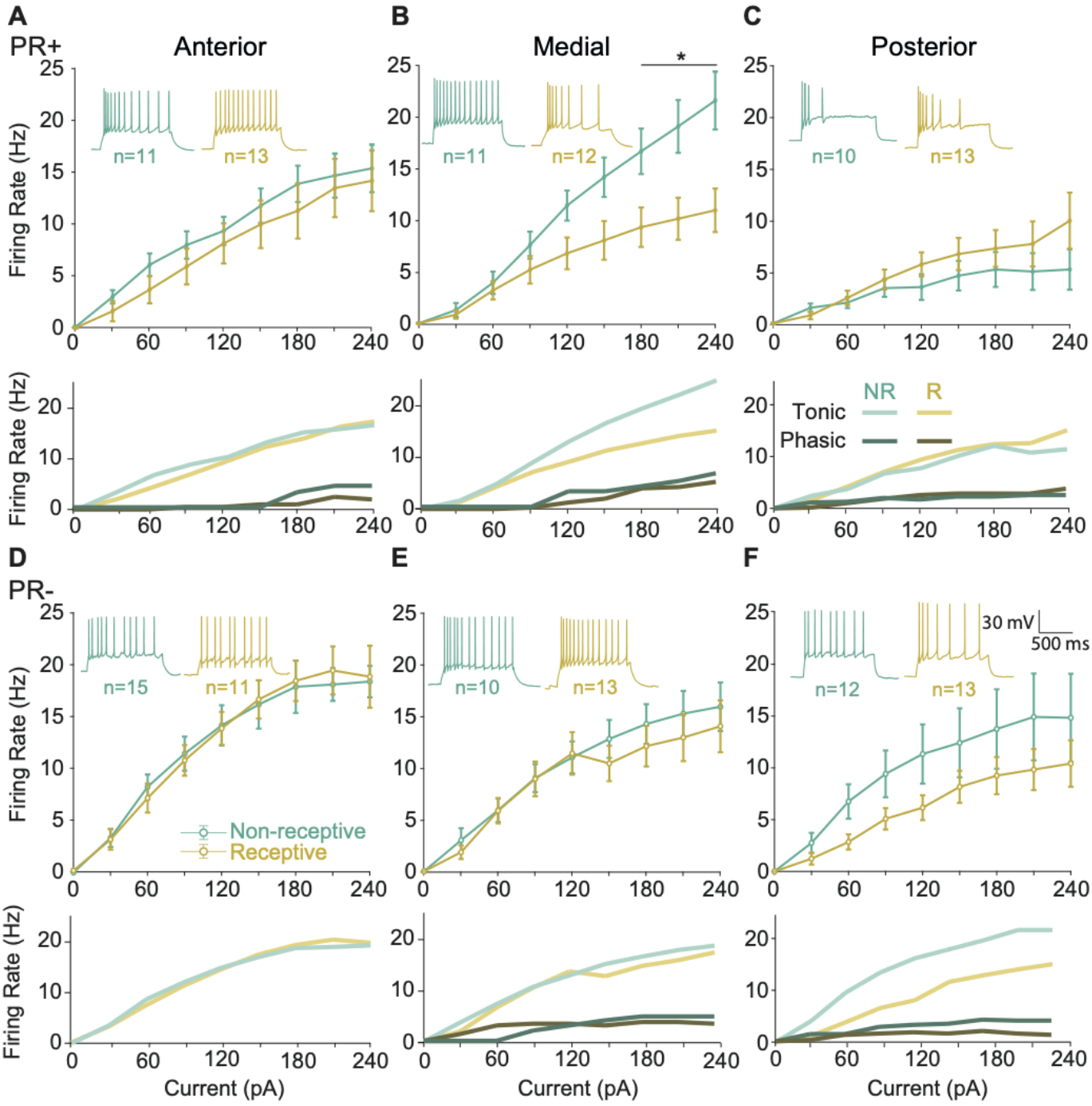

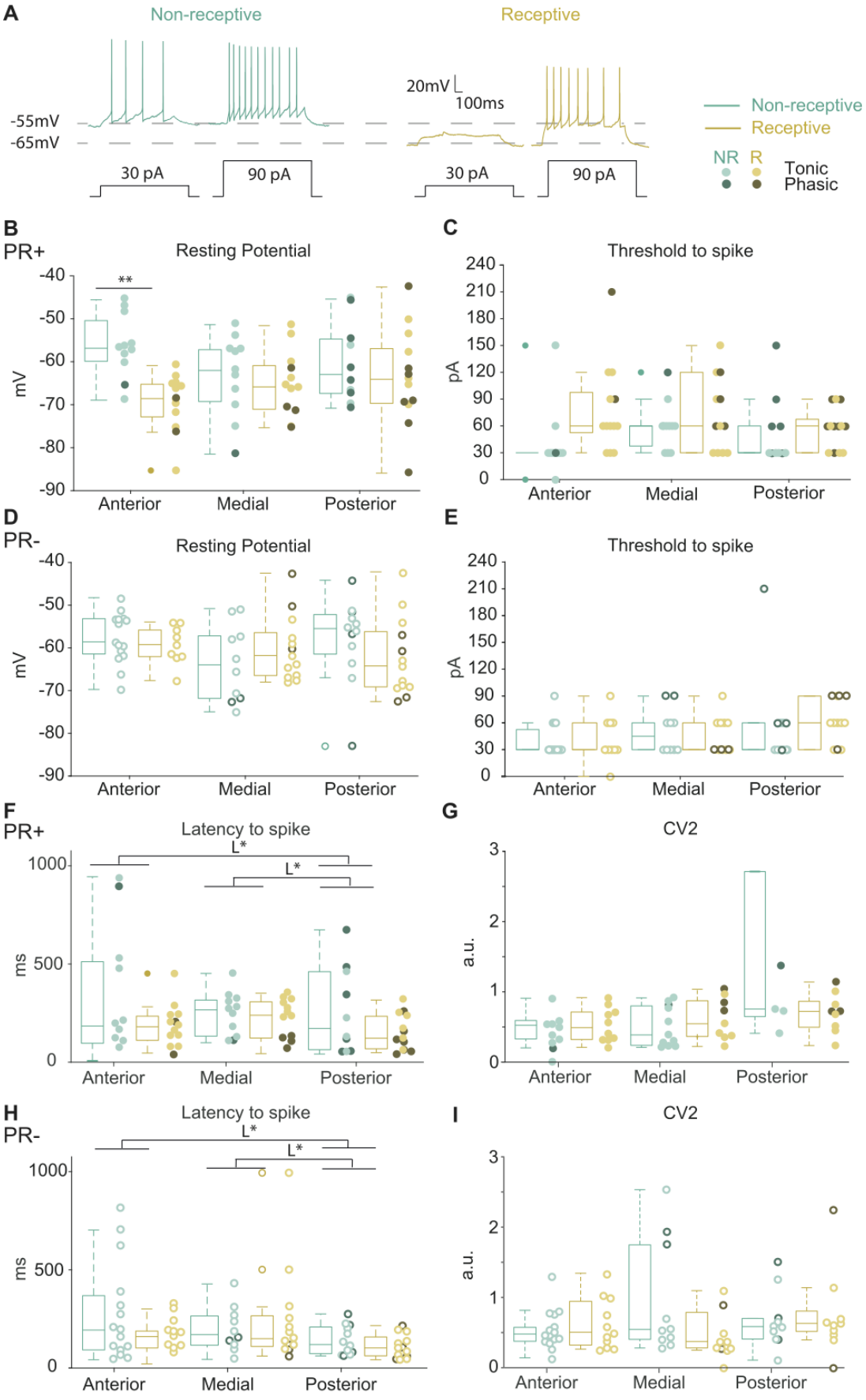

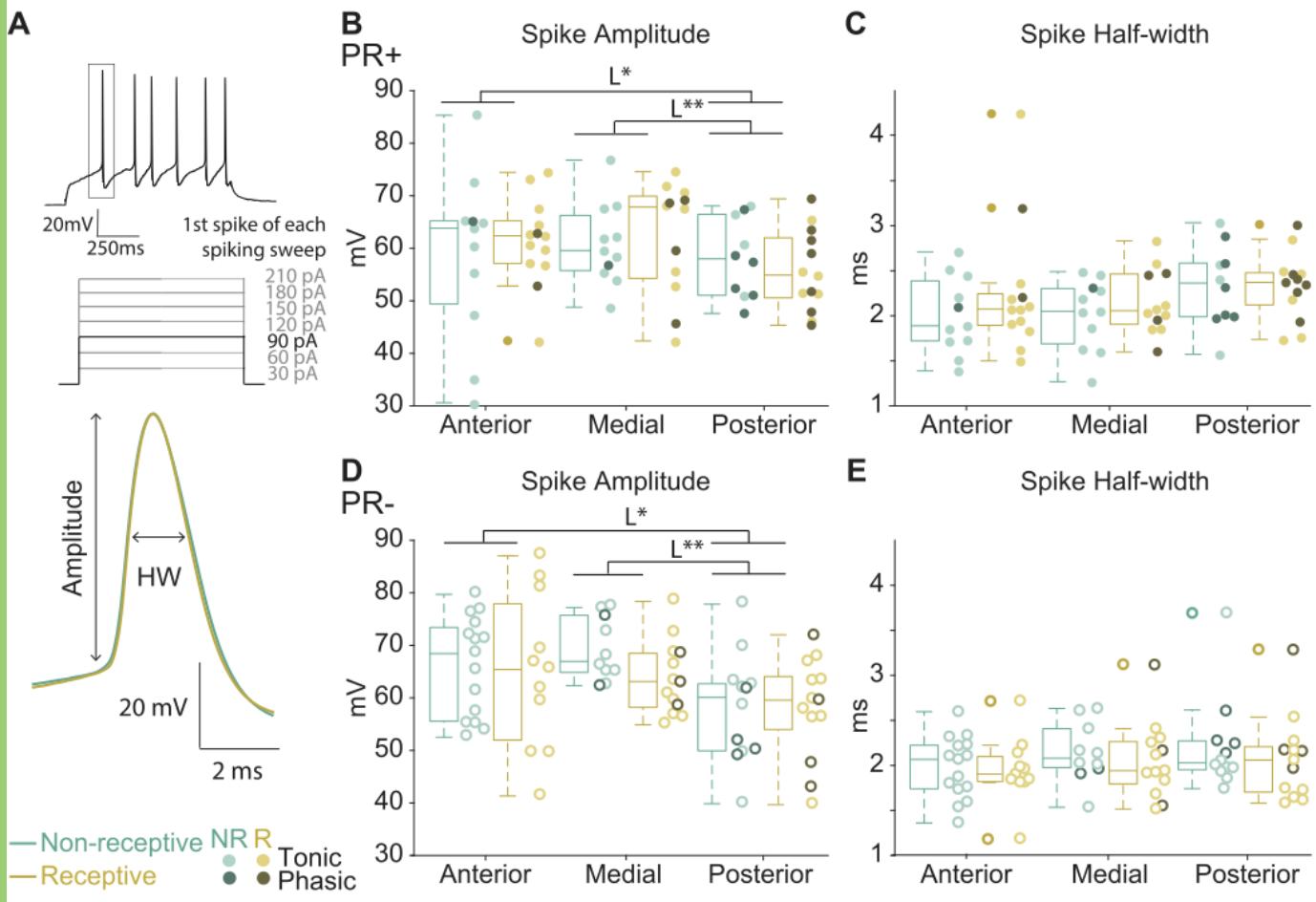

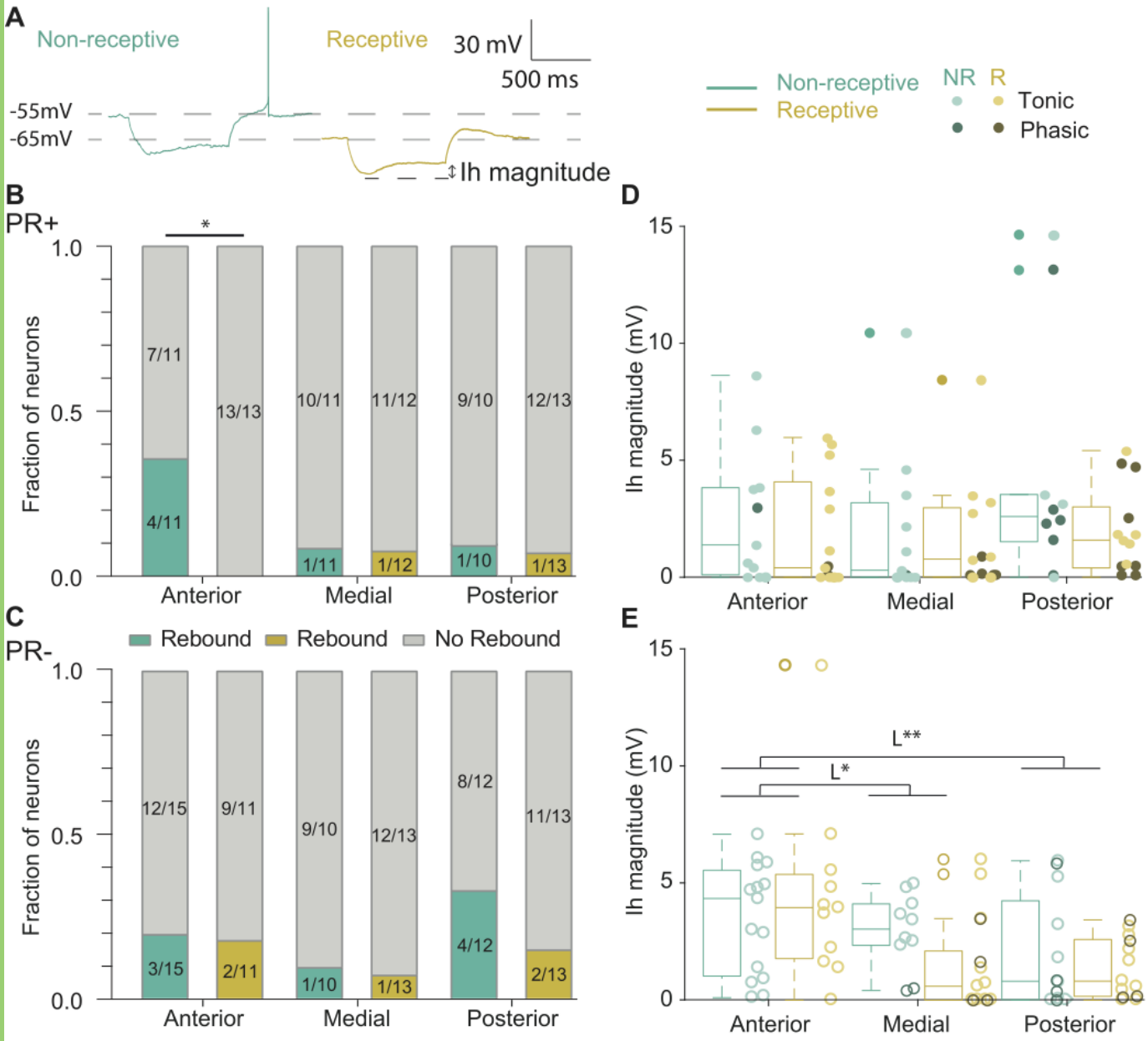

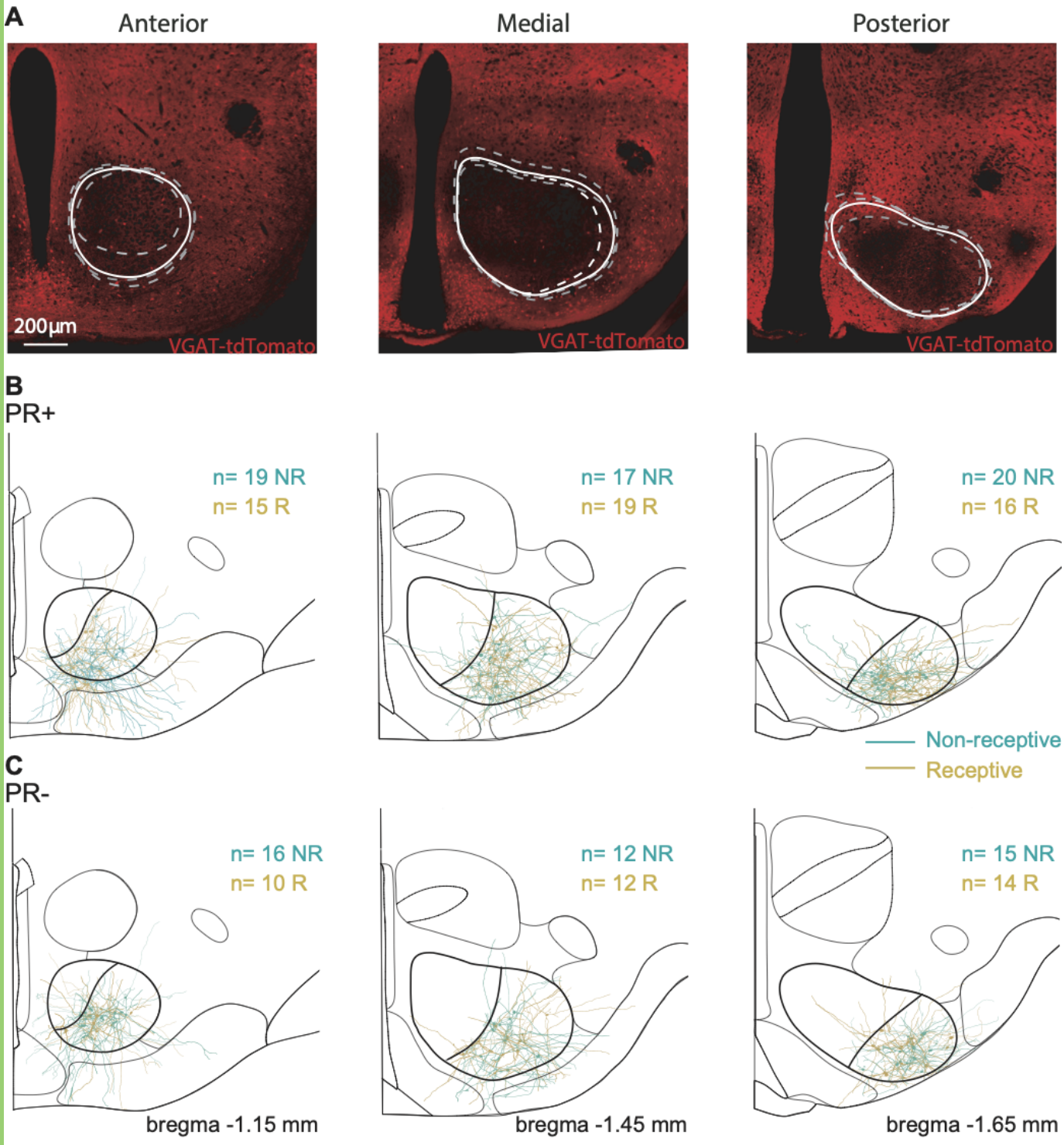

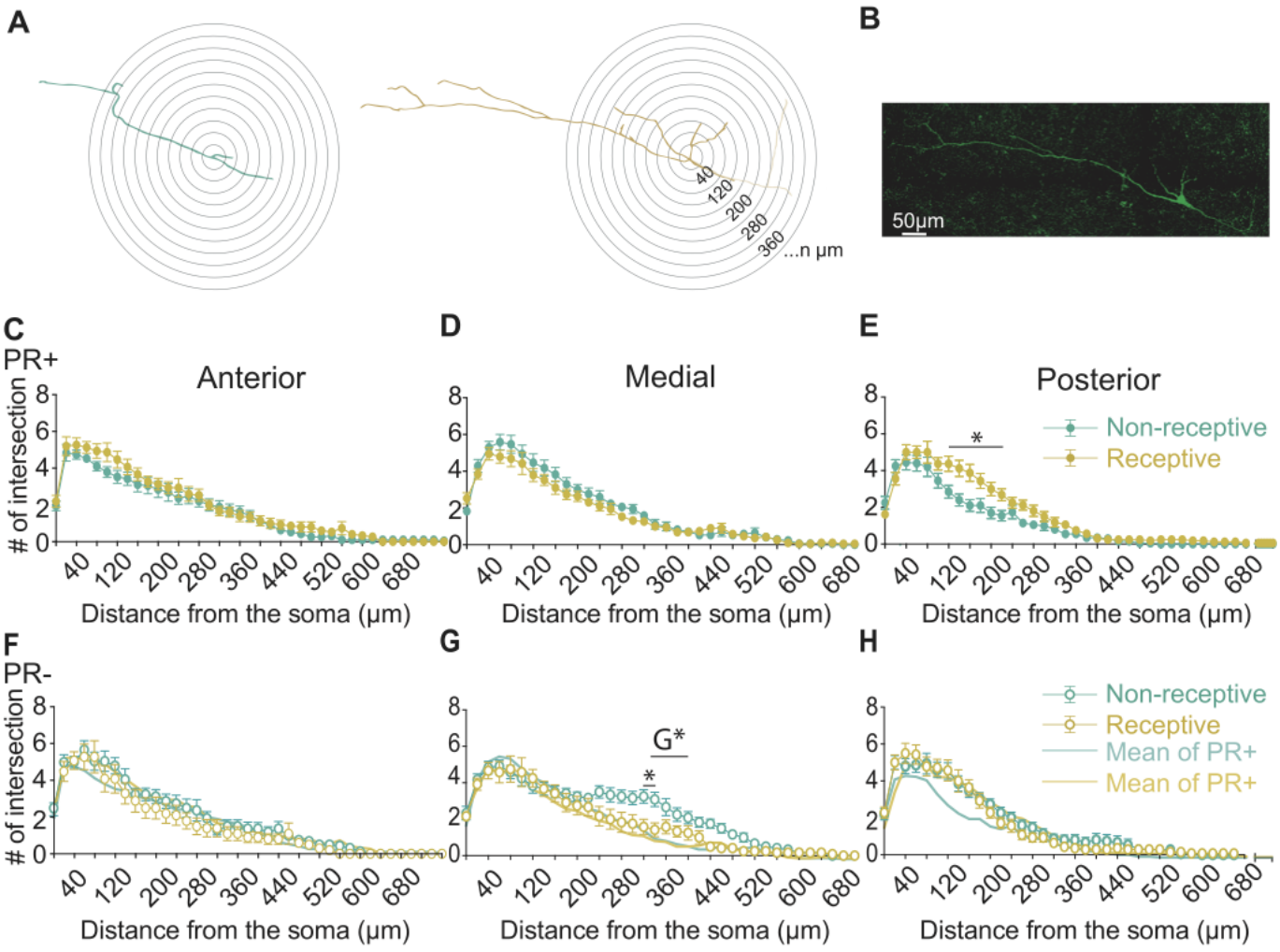

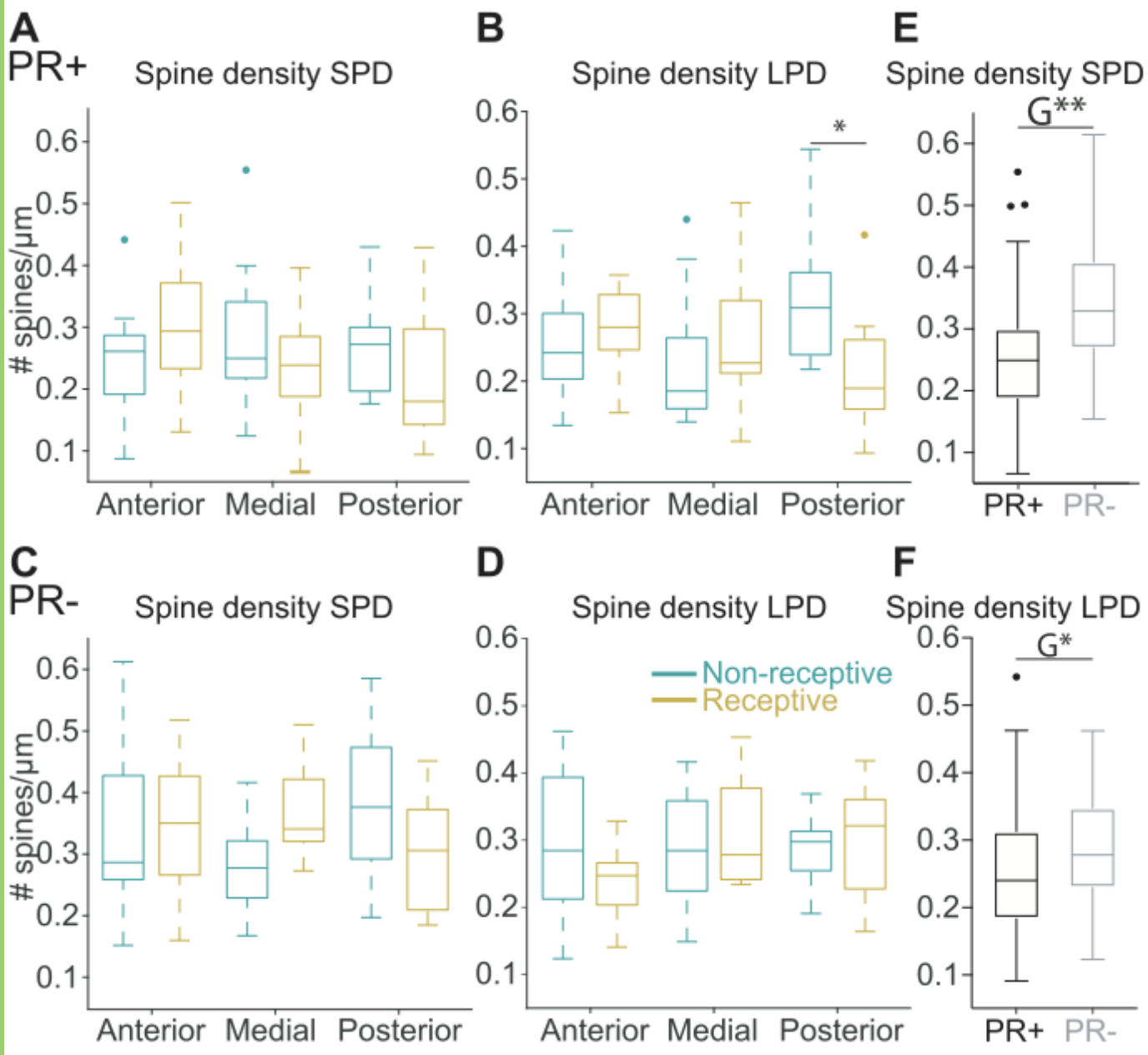

PR+ neurons

	Non-receptive						Receptive					
	Anterior (n=10)		Medial (n=8)		Posterior (n=11)		Anterior (n=9)		Medial (n=11)		Posterior (n=11)	
	T	P	T	P	T	P	T	P	T	P	T	P
Capacitance (pF)	9.03 (2.31)		11.57 (2.66) L1*		7.34 (5.02) L1*		11.45 (3.04)		10.04 (2.256) L1*		9.57 (2.70) L1*	
	9.08	8.99	11.59	7.83	8.21	7.34	11.45	9.87	10.04	9.26	9.57	10.17
Membrane Resistance (MΩ)	970.64 (1012.68)		788.77 (384.09)		912.00 (1209.69)		998.98 (604.43)		823.46 (853.00)		1082.56 (687.92)	
	1017.11	570.19	744.54	1231.50	999.65	912.00	998.98	1326.90	724.09	1116.09	995.93	1082.56
Time Constant (ms)	0.31 (0.09) L2*		0.36 (0.16)		0.22 (0.08) L2*		0.36 (0.18) L2*		0.27 (0.20)		0.24 (0.16) L2*	
	0.32	0.28	0.36	0.18	0.24	0.20	0.34	0.42	0.26	0.27	0.30	0.23

PR- neurons

	Non-receptive						Receptive					
	Anterior (n=16)		Medial (n=10)		Posterior (n=10)		Anterior (n=11)		Medial (n=11)		Posterior (n=13)	
	T	P	T	P	T	P	T	P	T	P	T	P
Capacitance (pF)	11.04 (4.70)		10.05 (1.89) L1*		8.82 (2.53) L1*		10.54 (2.90)		9.54 (1.28) L1*		10.53 (2.20) L1*	
	11.04	-	10.54	8.69	8.82	8.71	10.54	-	9.53	10.02	10.16	11.60
Membrane Resistance (MΩ)	808.55 (438.933)		1025.83 (425.53)		861.21 (284.09)		1258.25 (1412.35)		884.96 (654.043)		871.47 (556.16)	
	808.55	-	1142.86	781.92	873.94	861.21	1258.25	-	888.20	884.96	830.55	1160.18
Time Constant (ms)	0.36 (0.19) L2*		0.34 (0.18)		0.35 (0.17) L2*		0.36 (0.08) L2*		0.30 (0.11)		0.28 (0.16) L2*	
	0.36	-	0.38	0.23	0.34	0.37	0.36	-	0.29	0.34	0.28	0.32

PR+ neurons

	Non-receptive			Receptive		
	Anterior (n=19)	Medial (n=17)	Posterior (n=20)	Anterior (n=15)	Medial (n=19)	Posterior (n=16)
Soma area (μm^2)	184.88 (68.97)	217.01 (95.72)	193.08 (53.31)	219.77 (75.28)	182.92 (38.98)	219.31 (53.94)
Dendrites/neuron	7.00 (2.00)	7.00 (3.00)	6.00 (3.50)	7.00 (3.00)	9.00 (3.00)	7.50 (1.00)
Primary dendrites/neuron	4.00 (1.00) *L1**	4.00 (1.00) *L1**	3.50 (1.00)	4.00 (1.00) *L1**	4.00 (1.00) *L1**	3.50 (1.75)
Branch points/neuron	3.00 (2.00)	3.00 (3.00)	3.00 (3.00)	4.00 (3.00)	5.00 (4.00)	4.00 (1.75)
Dendritic length of LPDs	572.69 *L2** (199.05)	448.43 *L2** (268.22)	337.53 *L2** (287.65)	640.69 *L2** (277.72)	473.32 *L2** (273.33)	482.57 *L2** (202.10)
Average dendritic length of SPDs	205.36 (102.82)	214.50 (65.76)	145.53 (93.24)	181.54 (71.97)	170.55 (77.82)	177.85 (75.57)

PR- neurons

	Non-receptive			Receptive		
	Anterior (n=16)	Medial (n=12)	Posterior (n=15)	Anterior (n=10)	Medial (n=12)	Posterior (n=14)
Soma area (μm^2)	183.64 (58.52)	208.24 (66.82)	171.12 (105.02)	177.00 (124.49)	188.30 (112.71)	184.28 (68.46)
Dendrites/neuron	8.00 (4.00)	7.50 (3.50)	7.00 (3.00)	7.00 (1.50)	7.00 (2.50)	7.00 (2.75)
Primary dendrites/neuron	4.00 (1.75) *L1**	3.00 (1.00) *L1**	4.00 (2.00)	3.50 (2.25) *L1**	3.00 (0.75) *L1**	4.00 (1.25)
Branch points/neuron	4.00 (5.50)	4.00 (3.50)	3.00 (2.00)	3.00 (3.25)	4.00 (1.00)	3.00 (3.25)
Dendritic length of LPDs	642.64 *L2** (235.57)	644.05 *L2** (96.20)	509.16 *L2** (253.81)	566.10 *L2** (352.88)	494.52 *L2** (289.21)	389.96 *L2** (194.99)
Average dendritic length of SPDs	155.87 (62.25)	255.72 (102.05)	172.95 (79.60)	124.89 (60.77)	150.58 (134.84)	176.90 (85.55)